Palacký University Olomouc

Joint Laboratory of Optics and Institute of Physics of the Czech
Academy of Sciences

MASTER THESIS

Jiřina Prokopová

Atmospheric calibration of the Cherenkov Telescope Array - an observatory to detect photons with highest energies

Supervisor of the master thesis: RNDr. Michael Prouza, Ph.D.

Study programme: N1701 Physics

Specialization: 1702T001 Applied Physics

Prague 2017

I declare that I carried out this master thesis independently, and only with the cited sources, literature and other professional sources.

I understand that my work relates to the rights and obligations under the Act No. 121/2000 Coll., the Copyright Act, as amended, in particular the fact that the Palacký University in Olomouc has the right to conclude a license agreement on the use of this work as a school work pursuant to Section 60 paragraph 1 of the Copyright Act.

In .... date ....   signature of the author

Název práce: Atmosférická kalibrace Cherenkov Telescope Array - observatoře pro detekci fotonů s nejvyššími energiemi

Autor: Jiřina Prokopová

Katedra: Společná laboratoř optiky a Fyzikálního ústavu Akademie věd ČR

Vedoucí: RNDr. Michael Prouza, Ph.D., Fyzikální ústav Akademie věd ČR

Abstrakt: Atmosférické kalibrace jsou nedílnou součástí astronomických pozorování. Výzkumná skupina na Fyzikálním Ústavu v Praze vyvinula malý robotický dalekohled FRAM. Tento dalekohled slouží k okamžitému monitorování oblohy, pomocí něhož jsme schopni získat parametry jako VAOD nebo Ångströmův koeficient a vytvořit tzv. extinkční mapy. Toto zařízení bude nainstalováno na obou budoucích observatořích CTA. Vzhledem k tomu že bylo zapotřebí přístroj otestovat před instalací na samotné observatoři, byl jeho prototyp postaven v Praze. Zde monitoroval atmosférické podmínky po 14 měsíců a v rámci této práce jsme zanalyzovali naměřená data. Získali jsme statický soubor hodnot parametru VAOD a zjistili jsme jejich střední hodnotu, která má velikost 0.24 ± 0.17. Dále jsme rozebrali všechny podezřelé případy a pomocí této analýzy jsme ověřili plnou funkčnost systému.

Klíčová slova: FRAM, CTA, atmosferická kalibrace, VAOD

Title: Atmospheric calibration of the Cherenkov Telescope Array - an observatory to detect photons with highest energies

Author: Jiřina Prokopová

Department: Joint Laboratory of Optics and Institute of Physics of the Czech Academy of Sciences

Supervisor: RNDr. Michael Prouza, Ph.D., Institute of Physics of the Czech Academy of Sciences

Abstract: Atmospheric calibrations are integral part of astronomic observations. Research group at the Institute of Physics of the Czech Academy of Sciences in Prague have developed a small robotic telescope FRAM for rapid atmospheric monitoring, estimation of VAOD and Ångström coefficient and creation of maps of extinction. This device is planned to be installed at both of the future CTA sites. There was need for instrument testing before departure and therefore a prototype of this telescope has been setup in Prague. It has been monitoring astronomic conditions in Prague for about 14 months and we analyzed the acquired data within this thesis. We obtained a set of VAOD values with mean value 0.24 ± 0.17. We examined suspicious cases and ultimately verified full functionality of the system.

Keywords: FRAM, CTA, atmospheric calibration, VAOD

Contents

Introduction

Humankind has always been interested in phenomena and processes which take place in space and it already came a long way since it first looked upon the stars. Today, we are able to understand a great deal of natural phenomena but there is always much more to know and there are parts of universe which remain mysterious.

Direct research of the outer space is possible only partly through probes or spacecrafts and rovers in our Solar System. We got a large part of our knowledge just by studying spectrum of light incoming from space. We were able to exploit every part of electromagnetic spectrum for this task. In the last couple of decades we started to study elementary particles which arrive to Earth. These particles are so called cosmic rays.

We learned that it is possible to detect them directly from the Earth's orbit and also from the ground using Earth's atmosphere as a calorimeter. These particles interact with molecules and fields present in the atmosphere and create showers of secondary particles. Such processes may produce light which is detectable by ground based observatories.

We learned that primary particles which can trigger shower like this can be much more energetic than any other particle accelerated by any man-made device. We presume that these particles carry information about space accelerators which are capable of such increase in particle energy and we want to learn more about them. Moreover, as the particle traverses through space, it interacts with other particles most often with microwave cosmic background which is present everywhere. If particle reaches specific energetic limit, it loses its energy very fast through these interactions. This tells us that some accelerating mechanism has to be in not so far distance from Earth, which interests us even more.

The more energetic the particles get, the less intensive is their flux. Therefore, if we want to detect the most energetic of them, we have to cover a large area. This is something that cannot be done from space orbit and research must take place on the Earth's surface, where it is possible to build detectors which spread across hundreds of square kilometers. Breakthrough detection of very high energy photons was made by the creation of Imaging Atmospheric Cherenkov Telescopes and ultimately by stereo imaging, which is the technique they use. By detecting secondary shower from multiple spots, it is possible to create its three dimension reconstruction and determine e.g. arrival direction of primary particle. Great observatories like H.E.S.S., MAGIC and VERITAS are on the forefront of the current research. And now, construction of new big observatory is planned. It will be called Cherenkov Telescope Array or CTA and it should achieve set of ambitious goals and help us understand stated processes even better. It will be built at two sites, one at each hemisphere, and it will use three classes of telescopes according to the energy range they intend to detect. It is going to use all available information we have so far in order to tailor all its parts for a successful monitoring of photons of the highest energies.

As was mentioned, this means that the atmosphere will become an integral part of the detection mechanism, but it creates some obstacles as well. The atmosphere allows us to realize our measurements, but is also the source of problems

and uncertainties. If we want our detection to be successful, we have to understand and measure the atmospheric parameters. This way, we will be able to capture all changes which are happening there and monitor them. We can use this data for later calibration or we can make on the fly decisions and choose which part of the sky we want to observe.

There are several instruments which are able to measure certain parameters of the atmosphere like weather stations, infrared cameras, photometers and LI-DARs. It is considered to be advantageous to have an abundance of this kind of information and compare and confront them together. As it happens, every one of them has some advantages and disadvantages. Research group at the Institute of Physics of the Czech Academy of Sciences in Prague found there is a space for improvement and designed and constructed Photometric Robotic Atmospheric Monitor abbreviated as FRAM.

FRAM is basically a small optical telescope which monitors the sky during observations. It measures the light flux coming from the stars and compares them to their values from star catalog created by decades of astronomical observations. In this manner, it can evaluate light which was lost by its transit through the atmosphere. This loss is characterized by the extinction coefficient or parameter called vertical aerosol optical depth.

FRAM was used for a rapid atmospheric monitoring at the Pierre Auger Observatory in Argentina and will be built at the CTA sites. Its main purpose at CTA sites will be to create maps of extinction and VAOD measurement. Research group at Institute of Physics of the Czech Academy of Sciences in Prague aimed to improve its functions and is still working on data fitting and modeling. Before instrument departure to the CTA sites, FRAM prototype has been installed at the Institute premises for testing and control of all functions.

FRAM monitored atmospheric conditions at Prague for about past year and gathered many thousands of images that need to be processed and analyzed. Our task is to obtain VAOD values from these measured data and compare them to the values we already have from Argentina. We expect these values to be higher because atmospheric conditions in Prague are much worse compared to those at the Pierre Auger site or in the future at the CTA sites. Furthermore, we want to examine any suspicious values to exclude possible malfunction.

1. Detection of photons with the highest energies

Cosmic and gamma rays reach Earth every minute of every day from every direction. These high energy particles interact with nuclei in Earth's atmosphere and may produce cascades of secondary radiation called air showers [37, chapter 1.2.]. In this case the atmosphere serves as a calorimeter in which the shower can develop. However there are also other types of radiation that can be emitted during these collisions. When nitrogen molecule is hit by the incoming cosmic ray particle, it gets into excited state, and during the de-excitation part of its energy is isotropically emitted in the form of fluorescence radiation [33, chapter 9.6.6]. And when charged particle travels faster than light does in the atmosphere, it produces Cherenkov radiation [33, chapter 9.6.5].

Energy spectrum of primary particle behaves according to a diagram 1.2 from 10^9 eV up to 10^{20} eV. The more energetic primary particle, the more rare it is. Ultra-high-energy cosmic ray (UHECR), with energies of primary particle over 10^{18} eV, can cause cascade several kilometers long, i. e. so called extensive air shower (EAS) (further reading [37, chapter 7]).


Gamma shower   Hadronic shower
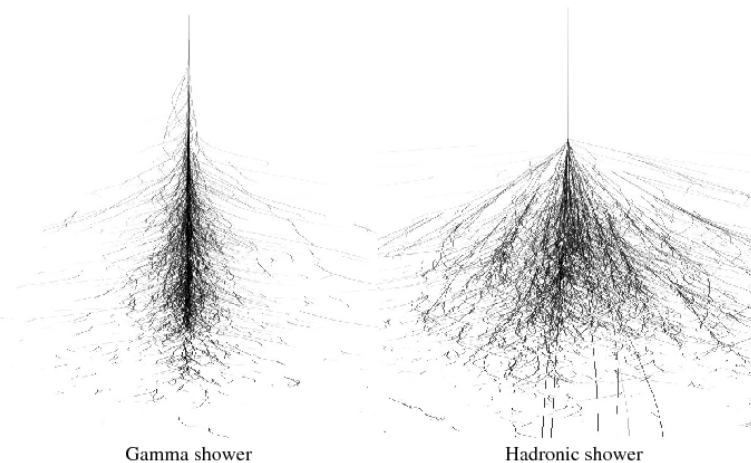
Figure 1.1: Difference in gamma and hadronic shower profile. Gamma shower is much more narrow and axially symmetric. Source: [40].

Properties of secondary showers are influenced by the type of primary particle. Nuclear cascades caused by protons are more penetrating and also wider, see 1.1. In case of photon the showers have only electromagnetic character. We refer to them as very high energy (VHE) gamma rays instead of EAS. [33, chapter 9.8.]

When particle such as proton travels through space it interacts with cosmic microwave background (CMB) radiation which is ubiquitous. During these interactions it loses its energy. For illustration of proton propagation trough CMB see 1.3. Nevertheless, it affects whole molecules such as helium, oxygen or iron in similar way. It was computed that if its energy is greater than roughly 5×10^{19} eV it is going to decrease quite fast, as can be also seen from the figure. This energy limit is named Greisen–Zatsepin–Kuzmin (GZK) cut-off [44] and quite fast in this case means that after approximately 100 Mpc it is going to drop to 10^{19} eV
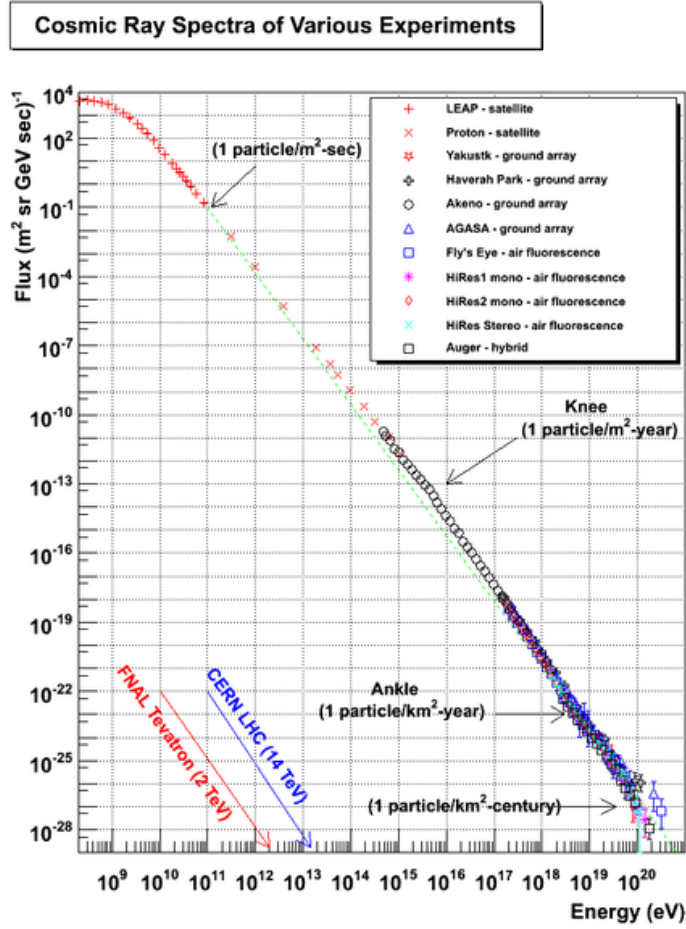
Figure 1.2: Energy spectrum of cosmic ray resembles a leg. Otherwise continuous spectrum deviates from its exponential decline (E $^{-3}$, see dashed line) in two areas: knee and ankle. Ankle is the part of the spectrum which covers UHECRs. Source: [37, chapter 2.6.].

again. It is clear that detecting any particle more energetic than this limit has to be rare and in the same time astonishing. It is worth mentioning that in 1991 experiment HiRes detected particle with energy more than 3×10^{20} eV, which is the record.

The figure 1.2 shows that by reaching energies around 10^{11} eV the flux of particles steeply decreases. VHE gamma rays with energies over 10^{20} eV are so rare that only 1 particle reaches 1 square kilometer of Earth surface in a century.

The rarest particles are very interesting for scientists, because they are tens of millions times more energetic than particles accelerated by any man-made mechanism. They carry information about accelerating processes in outer space and about the universe itself. By studying them, we may be able to figure out how such acceleration is possible and where it takes place.

In order to study them, we have to detect them and collect as much data as possible. In general, there are two methods of detection. Firstly it was established that due to its sparse flux we have to build vast network of detectors which will cover large areas of the surface. These detectors usually take form of tanks filled with e.g. water which has higher refraction index than air around. Secondary
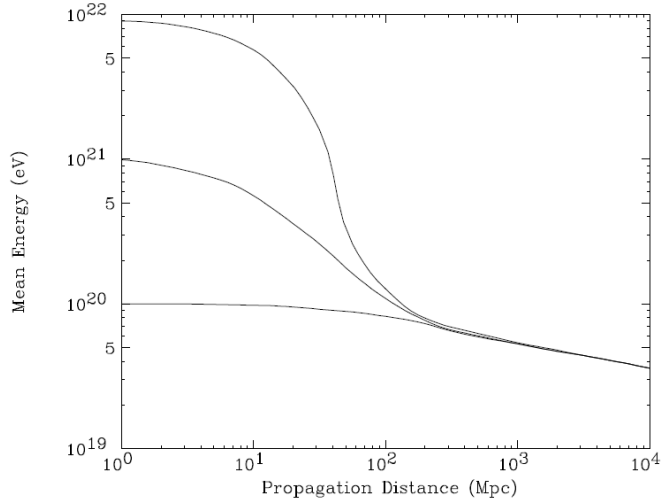
Figure 1.3: Illustration of GZK limit for protons. The figure shows their mean energy as a function of propagation distance. Source: [14].

particles with much smaller energy than the primary one that reach the surface are still energetic enough to produce Cherenkov radiation that we are able to detect with system of multipliers within the tank and sample the radiation. Secondly, we can take advantage of the emission of fluorescence or Cherenkov radiation that is already happening high in the atmosphere. For this purpose large telescopes produced of large reflector and photomultipliers have been built. Conveniently, it is possible to use combination of these techniques to get more accurate results.

Cherenkov radiation is key in case of detection of VHE gamma ray. Cherenkov radiation is blueish (or ultraviolet) light emitted by energy loss of charged typically relativistic particle which travels trough dielectric medium such as water or air with greater phase velocity than speed of light. One could say it is electromagnetic analogy of sonic boom. It is characterized by Cherenkov angle which is angle of incoming cone of Cherenkov light. The angle is at maximum when particle approaches speed of light. Further reading [42]. There have been already built ground-based detectors for this purpose called Imaging Atmospheric Cherenkov Telescopes (IACTs). There are currently three major IACT projects: H.E.S.S., MAGIC and VERITAS. They are all very modern observatories and are results of collaboration of many institutions and nations.

1.1 Gamma-ray Astronomy

Gamma rays are produced by variety of known and unknown sources. Unlike cosmic rays they are not affected by electromagnetic field in the universe and therefore travel more straightforward and we might be able to find space accelerators by tracking them.

We can say that there are three types of gamma radiation throughout the universe. The most common and least interesting is random background caused by diffused photons originating in our Galaxy. The others are galactic and extragalactic point-like sources and gamma ray bursts (GRBs).

Point-like sources refer to those who are steady and emit this kind of radiation
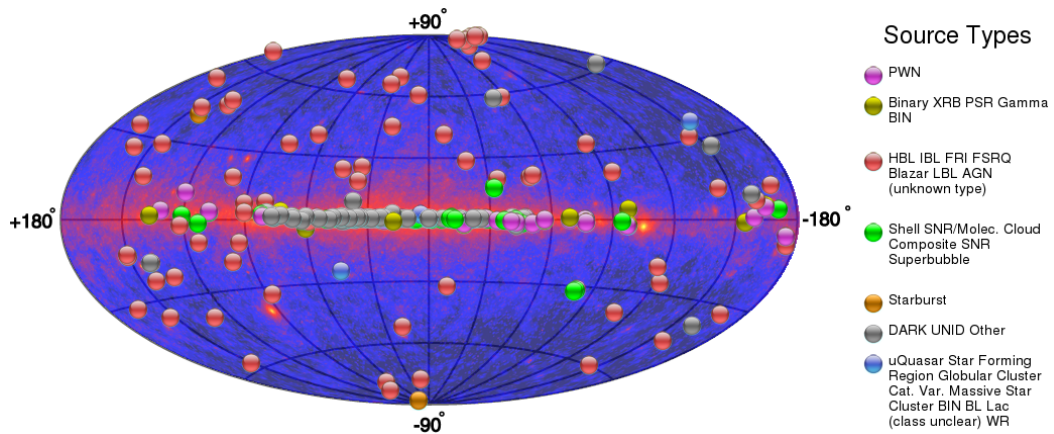
Figure 1.4: GLAST/Fermi Skymap of our Galaxy with marked detected sources. It shows extensive background in galactic plane, typical for gamma spectrum. Source: tevcat.

for a long time. Amongst production candidates are pulsars (PSR), supernova remnants (SNR) or quasars and active galactic nuclei (AGN). Hundreds of rotating neutron stars or pulsars have been discovered via radio astronomy but tens of others have been discovered recently using gamma astronomy. In general, these sources stand out from the background due to their high fluxes. Typical example is Crab nebula and it is even used as a scale for others. Next possible sources might be (super)massive black holes inside AGNs. Supernova remnants are vast relicts of star explosions. They are considered to be major candidates for cosmic ray acceleration. Such objects have very strong magnetic field which produces high energy electrons. These electrons are further able to boost surrounding photons due to inverse Compton effect. This thermal radiation is caused by heated falling matter. AGNs can also emit nonthermal radiation in form of jets of material accelerated to relativistic speed. In other words, these kind of sources can only be objects so massive it is behind comparison of anything we can encounter or observe in our Solar System [33, chapter 9.10], [33, chapter 8].

Gamma ray bursts are very intensive short flashes of gamma radiation. They were first discovered in 1960 by Vela satellite which purpose was to detect gamma rays from nuclear bomb blasts during Cold War. Today we are able to detect couple of them a day. There are two categories of GRBs. Long-duration witch period 2-10 s and short-duration, which last less than 2 s, specifically 0,3 on average. Unlike point sources its distribution seems to be uniform, their light curves differ and they occur in random directions. Long-durations bursts are associated with stellar collapses or collapsars. These events are caused by stars with 20-100 times bigger then Sun. It is believed stars that massive would collapse directly into black holes, releasing tremendous amount of energy in the process. Short-duration bursts are less frequently observed and therefore less understood. However, it is clear that their sources have to be incredible impact objects. It is believed they have different progenitors but with similar accelerations mechanism [33, chapter 9.11], [33, chapter 8].

1.2 Imaging Atmospheric Cherenkov Telescopes

Unlike charged particles photons fly trough space without significantly changing their direction. They are not affected by electromagnetic or any other force except for gravitation. That makes them suitable candidates for research and study because they can lead us to places in the universe where particles are accelerated to great degree.

The existence of gamma rays was expected and predicted. The research itself started, as it often happens, by accident. In 1952, was Mr. Blackett performing an experiment designed to investigate liquid scintillators. As 'collateral damage' he detected Cherenkov radiation in the liquid. This led him to the idea that it might be possible to detect the radiation in air. Not long after that first improvised ground-based telescope was born. Its mirror had only 25 cm and it was set up together with 5 cm photomultiplier in garbage bin. Luckily 1-2 pulses per minute were successfully detected.

This 'accident' had happened in right time because of a conference in Moscow few years later. At the conference, there has been set a goal to pursue high gamma ray point sources. Several projects followed. The first one in Russia, other in Ireland. They basically only proved first estimations of high gamma ray flux to be too optimistic. Collaboration between Ireland project and Smithsonian Astrophysical Observatory led to establishment of Whipple telescope in 1982, which represents second generation of ground based telescopes. It was functional for 20 years, found first convincing sources and made full scan of northern sky. However, at this stage of development there was not enough funding to make progress in ground based detection [21, section 2].

Spaced based detection program started in 1961, when the first gamma ray telescope was carried by Explorer XI satellite to Earth's orbit. The idea is that one can detect the primary flux directly and does not have to deal with extinction in the atmosphere. In following years, more satellites had been sent by NASA and ESA. They used scintillators like gas chambers and calorimeters for detection. As part of NASA's Great Observatories project CGRO (Compton Gamma Ray Observatory)[1] was launched. Its detector EGRET[2] uses inverse Compton scattering and it executed first sky survey and detected large number of potential sources, including extragalactic ones. On the other hand, the BATSE detector detected about 1 gamma ray burst per day and provided quick alert for ground based detectors (this type of detection was later carried on by Swift satellite in 2004). The most sophisticated and fruitful is Fermi gamma ray satellite which operates since 2008. Its LAT detector (EGRET successor) provides us with full sky scan every three hours. The second instrument GBM detects gamma ray bursts using 14 scintillators [27], [21, section 3], [33, chapter 9.10], further reading [37, chapter 8].

Although it is possible to detect primary radiation from space, we need larger collecting area in order to study VHE gamma rays (see figure 1.5), as we clearly stated above. Second generation of ground based detectors have had some issues. In order to move further in the research,[3] it was necessary to separate signal

---

[1]Learn more at [30].

[2]Learn more at [31].

[3]Some groups continued research with more advanced first generation telescopes. Using
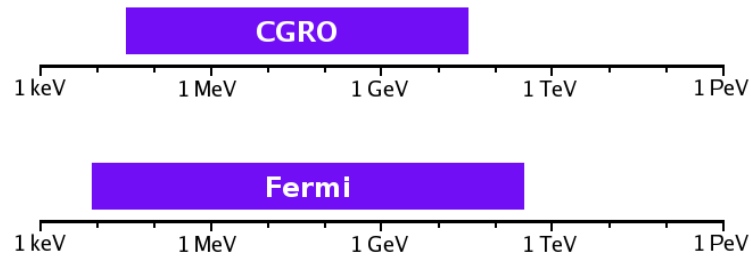
Figure 1.5: Detectable energy spectrum of space based telescopes CGRO and Fermi. May be compared with 1.9. Source: [27].

from sky noise caused by cosmic ray. Another problem was to identify Cherenkov flashes created by muons, which could be mistaken for studied signal.

It was clear that it is useful to study light distribution and lateral profile of Cherenkov radiation. When gamma particle enters the atmosphere, particles cascade spreads around its axis. In other words, it creates light cone, whose angle expands as it approaches the surface. By doing so, it uniformly illuminates area on the ground called light pool, see 1.6.
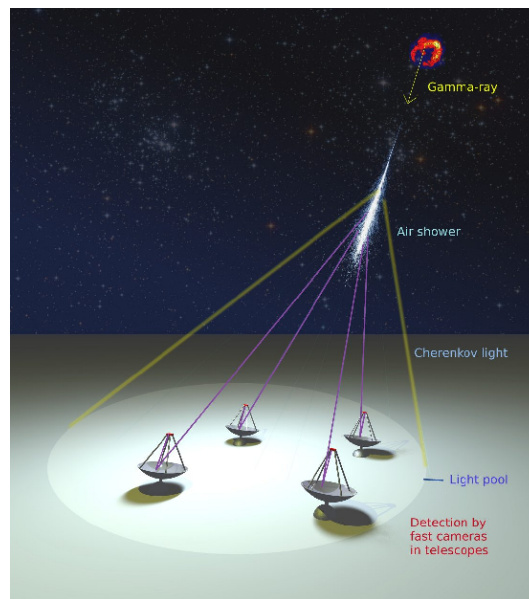
Figure 1.6: Schematic of Cherenkov light illuminating detectors. Source: [40].

This realization led to an idea of observing every shower from two (or more) different places. Through analysis of taken images we can derive intersection of its axes. This not only helps to eliminate parasite light but also determines source location, which is worthwhile. This approach is called stereoscopic observation.

If we detect or image the shower by four different detectors (similar to the figure 1.6), we mean to get four pictures of the same shower. This allows us to reconstruct the shower and even get its 3D model, as illustrated in the figure 1.7. Imaging Atmospheric Cherenkov Telescopes (IACTs) are based on this method [21, section 4].

---

techniques like wevefront sampling, further reading [21, section 6]
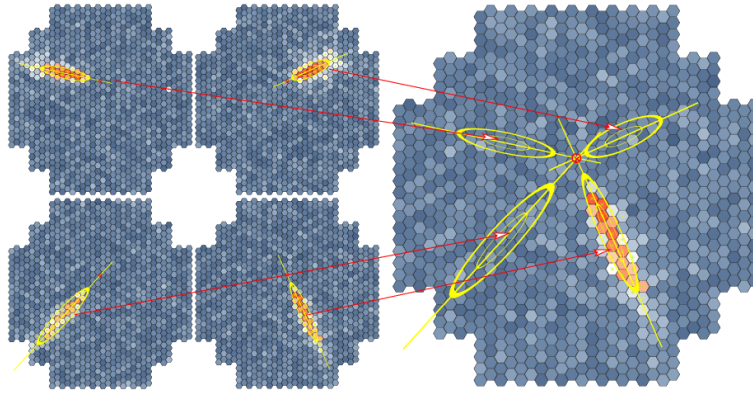
Figure 1.7: Schematic of shower reconstruction by stereo imaging. Source: [40].

Third generation is therefore represented by group of IACTs telescopes which enable simultaneous or stereoscopic observation of one shower. At this stage, computer simulations have become an essential tool. Whipple group performed a thorough observation of Crab Nebula.[4] Based on these observations they derived several empirical selection rules by studying shape and profile of showers. By applying this set of rules they have been able to clear the signal from distant noise and distinguish gamma ray induced showers from others. This type of research work is foundation of imaging telescopes [21].

Figure 1.8: Photographs of third generation telescopes: H.E.S.S., MAGIC and VERITAS. Source: [40], altered.

One of first big projects that have been 'upgraded' to third generation was HEGRA. After that, the most successful observatories so far followed: H.E.S.S.[5] in Africa, MAGIC[6] on Canary Islands and American VERITAS[7].

---

[4]Crab Nebula is a steady source that has been of interest since the Moscow conference in 1959 and which was successfully observed by several telescopes throughout the short history.

[5]More about H.E.S.S. observatory can be found on its website [11].

[6]More about MAGIC observatory can be found on its website: [12].

[7]More about VERITAS observatory can be found on its website: [13].

1.2.1 H.E.S.S.

H.E.S.S. observes southern sky[8]. It consists of four reflectors with segmented mirrors each with 108 m^2 mirror area and center one with more than 600 m^2. It allows simultaneous or stereoscopic observation of one shower [37, chapter 9.1.2], [21, section 7.2].
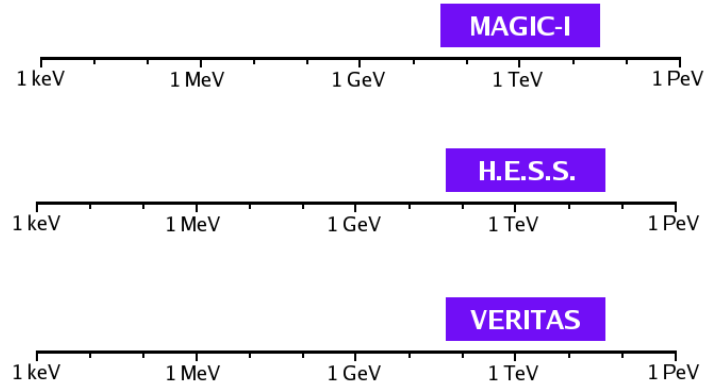
Figure 1.9: Detectable energy spectrum of IACTs: H.E.S.S., MAGIC and VERITAS. May be compared with 1.5. Source: [27].

It consists of four reflectors with segmented mirrors each with 108 m^2 mirror area and center one with more than 600 m^2. It allows simultaneous or stereoscopic observation of one shower. Over its course it detected tens of sources, including pulsars, stellar black holes and even found potential candidate for cosmic ray accelerator. The acronym which stands for High Energy Stereoscopic System cleverly pays tribute to Victor Hess, who discovered cosmic ray through his electroscopic measurements in hot air balloon experiment.[9]

1.2.2 MAGIC

MAGIC consists of two large 236 m^2 refractors today. However, its initial goal was to perfect non-stereoscopic observations by taking advantage of new technologies like avalanche photodiodes, more advanced cameras etc. and second telescope has been added only later. Among its contributions is for example idea of using time structure of the image in order to estimate displacement of the source [37, chapter 9.1.2], [21, section 7.1].

1.2.3 VERITAS

VERITAS is four telescope observatory. It was designed by Whipple group and build at Whipple Observatory in southern Arizona, just like the original telescopes. It also detected tens of sources[10], including first starburst galaxy. It

---

[8]Southern sky observed also Japanese IACT KANGAROO located in Australia [21, section 7.4].

[9]This discovery, for which he received Nobel prize, can be considered as beginning of experimental astroparticle physics, further reading [37, chapter 2].

[10]There are over 150 known sources overall.

studies pulsars, supernova remnants, gamma ray bursts and AGNs and even dark matter [37, chapter 9.1.2], [21, section 7.3].

1.2.4 Future

As we can see in figure 1.9 IACTs are capable of exploring higher energies of gamma rays than detectors in orbit (confront figures 1.5 and 1.9). Overall progress in getting to higher energies illustrates so called Kifune plot 1.10. Since we want to be able to detect even higher energies we need to increase sensitivity in this range. And as stated above, this can be done by increasing collecting area and therefore building larger projects. Today's best aspirant for this task is Cherenkov Telescope Array (CTA).
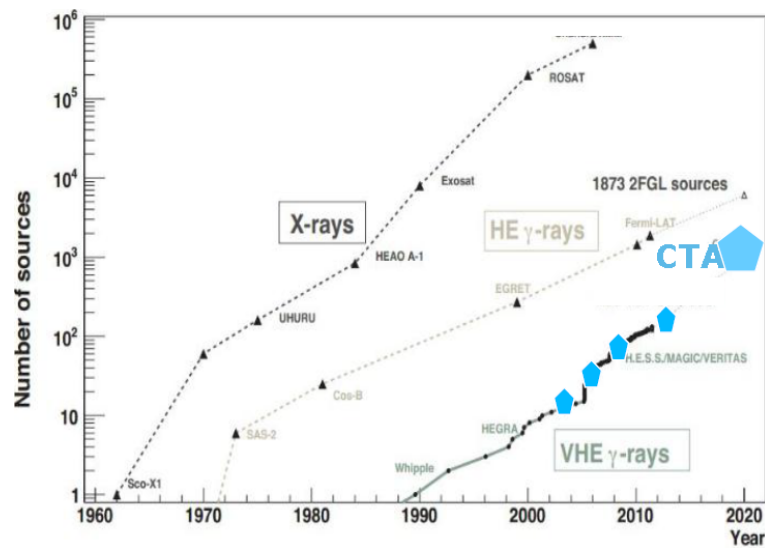
Figure 1.10: Number of sources discovered trough different wavebands over time. Similar diagram was first shown by T. Kifune in 1995. Here is also marked line for CTA. Source: [38], altered.

With IACTs scientist opened new window in the sky and started new branch of astronomy. CTA is the next logical step in the development of this branch [20].

2. Cherenkov Telescope Array

Cherenkov Telescope Array[1] is supposed to be representative of next generation gamma detectors. This projects takes into account all previous experiments listed above and it uses all existing data to create observatory capable of new discoveries.

Figure 2.1: Artistic illustration of CTA detection at night. Source: cta web.

The concept is a result of nearly worldwide cooperation of 27 countries and 160 institutions. It is designed to be open proposal-driven observatory which will provide easy access to observation and data analysis for wider scientific community [20].
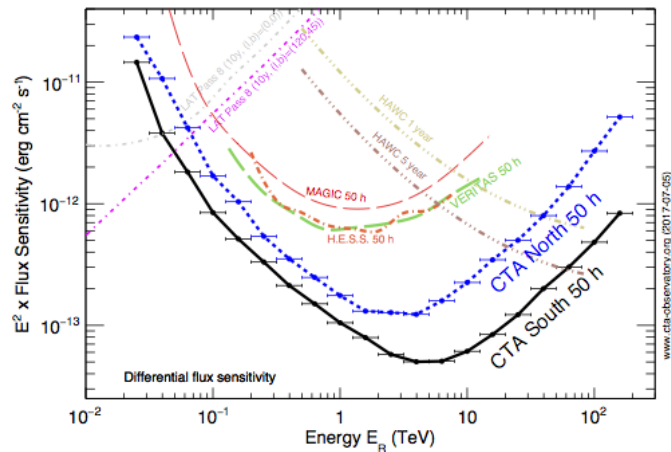
Figure 2.2: Comparation of third generation IACTs sensitivity with CTA's sites integral sensitivity from MC simulations. Source: [2].

It has many ambitious goals and potential to answer some questions about origin of relativistic cosmic particles, nature of dark matter and extreme environments like neutron stars or black holes. It may even discover brand new phenomena.

---

[1]More about CTA observatory can be found on its website [5].
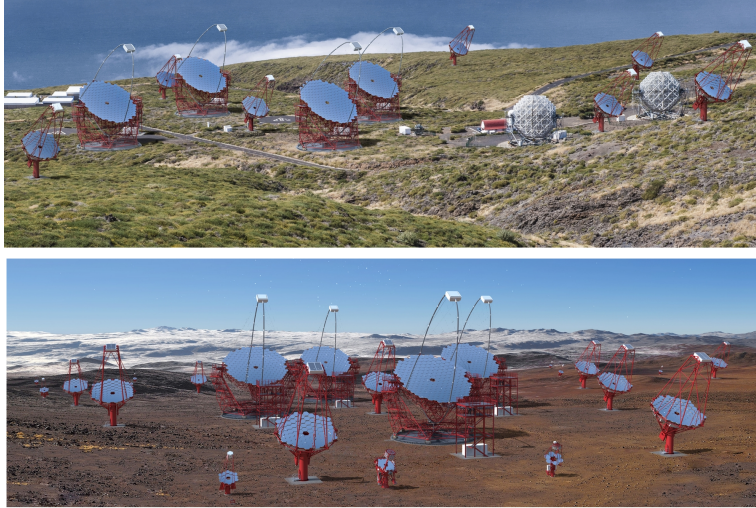
Figure 2.3: Illustrations of northern (above) and southern (below) sites. Source: [9].

One of biggest virtues is going to be full sky coverage, which is going to be achieved by detection at two different sites, one in southern and the other one in north hemisphere, see their illustrations in 2.3. It will probe the universe with sensitivity order higher than the previous generation did, see comparison in 2.2. Furthermore, it will have higher range of energy coverage (especially in south) from tens of GeV to several hundreds TeV, with better resolution in the core than before. As a result it will be possible to study known sources in much more detailed way and even discover new ones. It will improve the detection of extended sources due to wider field of view (FoV) and much better angular resolution.
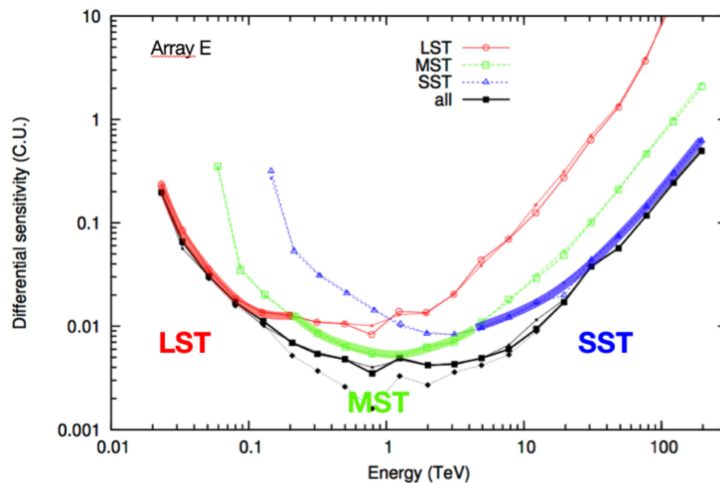
Figure 2.4: Sensitivity of individual classes of telescopes. Source: [2].

In order to cover all ranges of energy most effectively, three classes of telescopes will be available, see 2.5. Figure 2.2 can be modified to illustrate sensitivity of these individual telescope classes 2.4 in detail. Prototypes of every one of them are currently tested by different groups. Together they will spread across several square kilometers and therefore exceed present collecting area by far. This

improved temporal resolution allows CTA to detect frequent variations like blasts and flashes.

The Large-Size Telescope (LST) is meant to cover energy range between 20 and 200 GeV, thus low energies. These detectors have 23 m diameter segmented parabolic mirror. There are supposed to be four of them close to each other in every site.
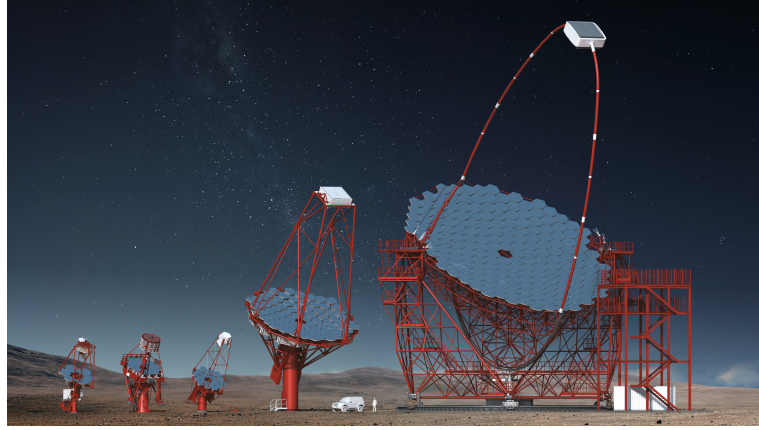
Figure 2.5: Proposed classes of telescopes. Source: [9].

Medium-Size Telescopes (MST)[2] will be 12 m in diameter and will cover core energies from 100 GeV to 10 Tev. 25 of them will be in southern and 15 in northern hemisphere. These higher energies spread over larger area, therefore they will not stand away from each other, with spacing around 100 m.

Smallest telescopes (SST) with the purpose of covering highest energies over 10 TeV, will stand even further apart (100 - 200 m) and also their number will be higher. 70 of them are planned for southern hemisphere. There still exist several prototypes. One of them ASTRI recorded its first Cherenkov light and took first image while testing, see 2.6.
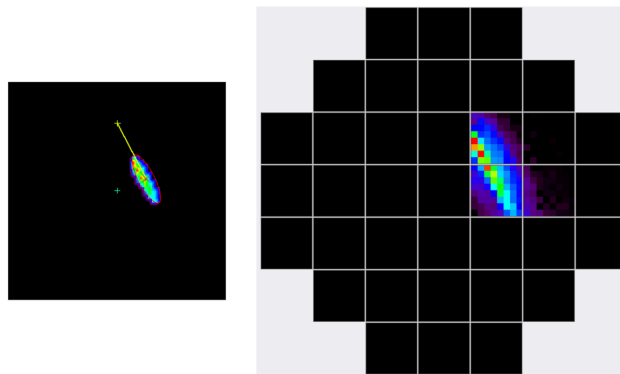
Figure 2.6: Prototype ASTRI's first image taken during the nights of 25 and 26 May, at the astronomical site in Sicily. Picture on the right shows sought event. Such image allows to reconstruct direction of primary particle, which is indicated by yellow line on the left picture. Source: [8].

---

[2]There is also high-performance version of MST called Schwarzschild-Couder Telescope (SCT).

Both future array sites have been carefully selected. Northern one will be located in La Palma, one of Canary Islands, near MAGIC telescope. In southern hemisphere the site will be located in Atacama Desert in Chille, 10 km southeast of ESO's Paranal Observatory. Southern site is going to focus on galactic sources, while northern one on extragalactic ones. You can see proposed layouts in following figure 2.7. Subset of telescopes will be able to operate independently, which increases flexibility.
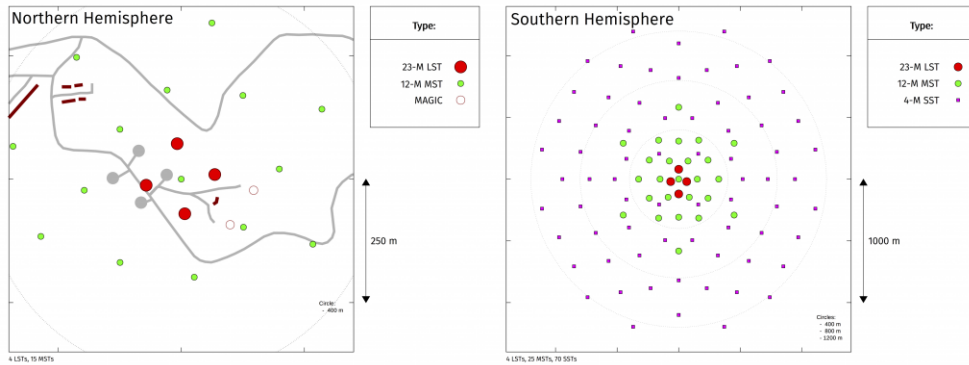
Figure 2.7: Proposed array layout for individual sites: north (left image) and south (right image). Source: [7]

As has been already said, the whole CTA design with all its parts is a result of cooperation of many institutions and more than 1000 scientists. It brings opportunity to study universe but that is not the only part of this research. Preparation and selection of the site, development of individual classes of telescopes - their design, their parts, their special mirrors, materials, electronics, interface, tools for data analysis, calibrations and so much more needs to be done. One of important subjects is also atmospheric calibration [2, 22, 20, 10, 7, 6].

3. Atmospheric Calibrations

3.1 Atmosphere

Interactions in Earth atmosphere are essential for particle showers evolution and emission of Cherenkov light. At the same time, the existence of atmosphere brings difficulties and uncertainties. One needs to understand processes which take place there in order to measure them effectively.

We divide our atmosphere to several layers according to their properties and phenomena that occur there. You can see their height distribution in figure 3.1. This picture indicates which layers gamma rays penetrate into.
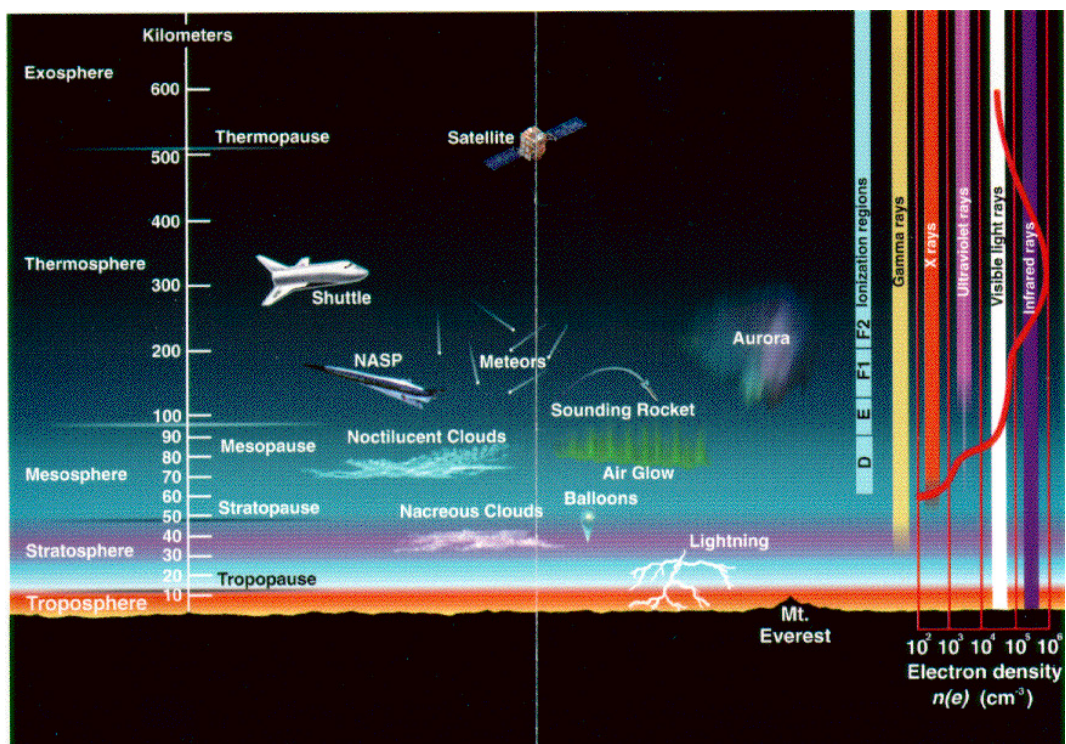
Figure 3.1: Atmospheric layers. Source: [32].

The most important layers for shower development are bottom layer named troposphere, in some cases also tropopause and lower layers of stratospere. Troposphere is the layer we live in and where most part of weather happens. It reaches from the surface up to 6 to 20 km depending on latitude. It is rich with aerosols and water vapor and their contribution constantly and significantly fluctuates [43].

Astronomical sites are carefully handpicked places with excellent atmospheric conditions, with high altitude, low humidity with minimum of rainfall and majority of clear nights, far away from human civilization which produces parasitic waves, vapor etc. Nevertheless, we cannot avoid nor prevent events which take place kilometers above the surface.

So far, the supplementary instruments at ICATS sites have been used only for quality maintenance. At some sites, there are now emerging efforts for monitoring

and consecutive data correction. It is clear there needs to be atmosphere extinction profile worked out. This means that computer modeling and simulations will once again play a key role in this part of research.

CTA has strict requirements about systematic uncertainties. Lower limit for existing instruments is 15 %, see 3.2. For CTA, this value should not be higher than 10 %. Most of residual systematics are caused by rapid changing of atmospheric conditions. The only way to achieve that is by carefully designed atmospheric calibration strategy[1], specifically tailored for CTA and its locations.

Part	Typical syst. uncertainty current instruments	Goal for CTA	remarks
10% systematic precision on the energy scale			
8.5% systematic precision on the atmospheric part			
Simulation codes	5%	1–2%	responsability of the MC working group
Simplifications in MC	2%	2%	responsability of the MC working group
Cherenkov light creation	5%	2%	energy-dependent, assessed by radio sondes and GDAS
Ozone absorption	3%	1%	seasonal variations, climate change, assessed by the spectrograph
Molecular extinction	2%	1%	assessed by radio sondes and GDAS
Cirrus layers extinction	5–10%	1–2%	assessed by LIDARs and FRAM (under optimal conditions, otherwise worse)
Boundary layer extinction	5–10%	1–2%	assessed by LIDARs and FRAM (under optimal conditions, otherwise worse)
Scattered Cherenkov light	<1%	<2%	affecting mainly SSTs, responsability of MC
Total	10–16%	4–5%	under optimal conditions, otherwise worse

Figure 3.2: Planned error budgets for CTA. Source: [10]

Integral part of this strategy is the use of different instruments and methods which enables cross-checking of acquired data. The ultimate goal is to create coherent weather monitoring, modeling and forecasting system. This system should ensure safety of instruments, provide informations for follow up corrections of observed data, help to make on-site scheduling decisions or target selections and record all data that could be possibly useful for final data analysis.

As we established above, atmosphere is in a way part of measuring system since it serves as calorimeter. After Cherenkov light emission it passes further trough the atmosphere and some of it is lost before it reaches detection system. The amount of lost light is called an atmospheric extinction. What is left is detected intensity and therefore an important characteristic for atmospheric calibrations [10, chapter 4.7], [22].

---

[1]Another ways to decrease residual systematics are camera calibrations, array calibrations and pointing calibrations localizations of point-like sources. Actual atmospheric calibration error budget is around 8 %, see 3.2.

3.2 Atmospheric extinction

Atmospheric extinction is caused by two fundamental mechanisms: scattering and absorption. Cherenkov photons might be scattered by molecules of air, which is called Rayleigh scattering, or by solid particles or liquid droplets, which is called Mie scattering. While molecules travel slow and their influence can be computed, liquid droplets or aerosols, which are plentiful in the troposphere, change fast and any subsequent correction is much more difficult. Weak flux of Cherenkov light may be absorbed solely by scattering. However, the true absorption is due to ozon, water vapor and oxygen present in the atmosphere.

In successful attempt to explain why is sky blue, Lord Rayleigh showed that the scattered intensity of light should be inversely proportional to the fourth power[2] of the wavelength of the light. At the same time, the intensity depends on refractive index of the air. We will call contribution from this kind of scattering k_{R}. In case of Mie scattering is the computation complicated by significant diversity between aerosol types and sizes. Nevertheless, for relevant range of size distribution the dependency is approximately inversely proportional to wavelength[3]. Analogically the contribution will be k_{M} The set of these influences affects Cherenkov angle and shower development itself. It also causes dimmer image due to photon loss and blurred one by photons backscattering into the camera [10, chapter 4.7], [36, chapter 5].

In general, we observe incoming light trough column of air, whose height depends on zenith angle or altitude. This column X is called airmass. Intuitively if we compare intensity of light before and after passing through the atmosphere, we will get the amount of extinct light.[4] This is best expressed with following formula:

$$m_{\mathrm{obs}} = m_{\mathrm{cat}} + (k_{\mathrm{R}} + k_{\mathrm{M}})X, \tag{3.1}$$

where m_{obs} is observed intensity of some star and m_{cat} its catalog value.

One of the founders of spectroscopy A. J. Ångström proposed a formula for spectral dependence of atmospheric extinction

$$\mathrm{AOD} = \beta \cdot \lambda^{-\gamma}, \tag{3.2}$$

the coefficient γ bears his name, β is turbidity (haziness) coefficient. AOD stands for aerosol optical depth. Today it is known that this formula is merely special case of more general one. Both γ and AOD is however often used to characterize aerosol extinction and therefore to quantify atmospheric profile [36, chapter 5], [26, 39].

Total optical depth (OD) characterizes medium through which radiation passes and it consists of aerosol optical depth (AOD) and optical depth caused by molecules predominantly given by Rayleigh scattering. We also recognize vertical optical depth (VOD) or vertical aerosol optical depth (VOAD) which presumes airmass to be equal to 1.

AOD or VAOD together with Ångström coefficient is considered to be standard quantity for characterization of atmospheric extinction. If we would like to

---

[2]Currently used value is 4.08 [36, chapter 5.1.1].

[3]More precisely, the power law is equal to -1.2. [36, chapter 5.1.1]

[4]Since we cannot measure original intensity of Cherenkov light, we need to use another light source for potential measurement purposes.

determine VAOD, firstly we need to know the difference between observed and catalog brightness of stars divided by airmass, through which the observation is done. Secondly, we need to convert this value from magnitude scale. This scale is logarithmic, which means that if some star is brighter by 5 magnitudes we receive 100 times more light from it. The conversion factor is therefore

$$\ln(\sqrt[5]{100}) \approx \ln(2.512) \approx 0.921.$$

After this step, we have to subtract molecular optical depth τ. Thus:

$$\text{VAOD} = 0.921 \cdot \frac{m_{\text{obs}} - m_{\text{cat}}}{X} - \tau_{\text{M}}. \tag{3.3}$$

3.3 Measurement and analysis of atmospheric parameters

Atmospheric analysis leads us to set of characteristics we need to measure. They are aerosol presence, molecular profile and individual extinctions, ozon absorption and Cherenkov light emission and scattering. We are also interested in atmospheric profiles like density, thickness, refractive index and optical depth. We must not forget basic weather conditions like temperature, humidity, wind etc.

3.3.1 Weather stations

Weather stations are widely used for measurement of basic characteristics. For similar purpose, air-balloon-based radio-sondes. At CTA sites there will be several anemometers for careful recording of the wind.

3.3.2 Clouds monitoring

Clouds contribute to atmospheric extinction due to their higher optical depth. To map cloud coverage all-sky (infrared), cameras may be used. Cloud altitudes may be additionally measured by ceilometers (infrared LIDAR). Such cloud analysis is useful both before and during actual measuring. It is possible to observe short-term changes and decisions about future target selection.

3.3.3 Photometers

One of long-term monitoring tools is Sun/Moon photometer. It is instrument for AOD measurement. It is more often used and better understood in its day-mode. Fortunately, it is also possible to use the Moon as the light source and measure AOD value and its development during the night.

3.3.4 LIDARs

Probably the most common instruments for aerosol estimations are LIDARs. LIght Detection And Ranging is tool for distance measurement. It principally consist of pulse laser, which is used to send light beam towards measuring object

Figure 3.3: Future CTA Raman lidars, currently in development by IFAE/UAB in Spain (left), LUPM in France (center) and CEILAP in Argentina (right). Source: [10]

and after this part of light is reflected back, it is detected using photomultipliers. It is possible to employ it for aerosol properties measurements in the same way using Raman scattering on nitrogen and oxygen. It is helpful to collect larger amount of data before observation itself. Knowing aerosol stratification allows us to run multiple Monte Carlo simulations for different atmospheric properties. It is not possible to use it directly during observation due to its invasive nature. At the same time, their usage is favourable, since they are able to detect both ground-level aerosols, and the vertical structure of higher altitude aerosols [10, chapter 4.7], [36, chapter 5], [18].

3.3.5 FRAM

An interesting way to obtain maps of atmospheric extinction is to use optical telescope FRAM. This device was successfully implemented at Pierre Auger Observatory and will be used at both CTA sites. Next chapter will be devoted entirely to this instrument.

There are some additional instruments that may be useful like lighting sensors and dust counters. Suitable software and interface are no less important.

3.4 Simulations
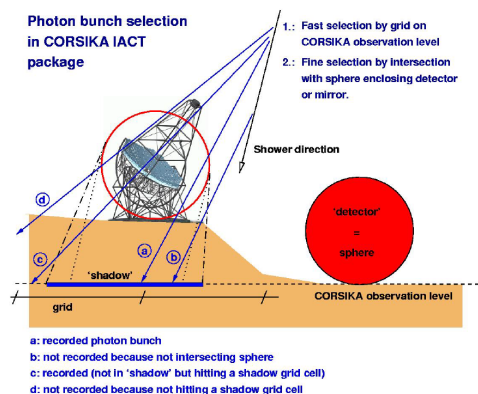
Figure 3.4: CORSIKA IACT package scheme. Source: [1].

All previous tools instruments provide us with atmospheric data. Besides actual data processing, it is also necessary to run good deal of simulations. In case of CTA, it is currently the key part of research since the project itself is in development. At this stage, many research groups rely on various simulations to help them develop and improve individual instruments and procedures.

The most important among them are Monte Carlo simulations, which are running on Europe-wide computing clusters Grid. CTA will be using program CORSIKA to simulate Cherenkov light emission. New option called IACT was recently developed for this purpose. In this option, the detector configuration is a 3-dimensional collection of spheres. However, it is possible to approximate to range of angles around shower axis, see 3.4. This software, which was extensively tested in the past, is publicly available and has a number of interaction model options. Another integral part is a detector response simulations program called sim_telarray. This program was developed for HEGRA, well established at H.E.S.S. and now improved for CTA [1, chapter 1], [41].

4. FRAM

The importance of atmospheric monitoring was clarified in previous chapter. Alongside existing instruments like weather stations, LIDARs, ceilometers or all-sky cameras, it appears to be favorable to have available non-invasive instrument which will measure cloudiness and aerosol content with sufficient sensitivity and resolution.

F/(Ph)otometric Robotic Atmospheric Monitor[1] or FRAM was created by the Institute of Physics of the Czech Academy of Sciences. FRAM is basically a small astronomical telescope. Its primary purpose is to provide information about atmospheric conditions and create maps of atmospheric extinction [25, 28].

Figure 4.1: Version of FRAM at the Pierre Auger Observatory. Source: [25].

The idea of building FRAM was based on a need for such information at Pierre Auger Observatory. As was said before, atmospheric conditions can sometimes change very fast and abruptly and it is helpful to have data for the actual time of observation. This kind of data can be used for on-the-fly scheduling decisions as well as for later analysis.

In its nature, FRAM is simply an optical telescope and when there is no need for atmospheric monitoring it can also be used to take photographs of deep-sky objects at a public request [36, 28].

4.1 Measuring principle

If we recall formula 3.1, we see that extinct light can be worked out by comparing observed light from stars with its catalog value. Star emmited light, which

---

[1]Apart from the acronym, was the device named after Norwegian ship Fram, that was build for polar expedition in 1893. The name means onward in Norwegian. They say that Fram have sailed further north and further south than any other wooden ship.

is coming to us from space, has to traverse greater path through airmass X than Cherenkov light which emerges from troposphere. This represents disadvantage of this method. Nevertheless, upper layers of our atmosphere are much more sparse and only minority of light extincts there.

In course of decades of observation, scientist gathered sufficient amount of data using different filters and techniques to create catalogs of stars observable from Earth along with their magnitudes. These catalog values are merely star brightnesses without contribution of atmosphere or influence of measuring instruments. Instruments may affect measurement and this influence is called instrument zero-point Z_i. Formula 3.1 thus transforms into:

$$m_{\mathrm{obs}} = m_{\mathrm{cat}} + Z_i + kX, \tag{4.1}$$

where k is the total extinction coefficient. In other words, k is the variable that interests us. The airmass X might be computed from series of measurements or standard models or seasonal models for specific area might be used [36, chapter 5.11].

FRAM selects standard field in its FoV and takes an image of it. Every image is then processed by star detection algorithm which chooses all standard stars with predefined properties. In accordance with the theory, it measures magnitude of those stars and compares it to their known catalog magnitude.

In order to achieve precise results, we need to consider many other effects, which influence our measuring process. Basically, we need to create a model to fit observed data.

We follow the equation 4.1 and add other variables. Firstly, we determine average color of light and we assign compensation constant for this color since blue light muffles more than red light[2]. New equation member then reads $c_1(B-V) \cdot (c_2(B-V)+1)$, where B and V are color indices and c_1, c_2 are constants for lower and higher order correction. Another necessary step is considering molecular scattering mentioned in the previous chapter. This is implemented by so called Rayleigh subtraction k_c which leads to following member: $k_c A(B-V)$ since it depends on airmass as well as on color of the light. Technical execution also requires several corrections. Next member $R_1 r(R_2 r+1)$ compensates inaccuracies caused by different distance r of the star image from the center of the image. Nonlinearity caused by imperfect reading from chip is characterized by M. After considering all these aspects, our current model is summarized in the following equation:

$$m_{obs} = Mm_{\mathrm{cat}} + Z_i + k_i X + c_1(B-V) \cdot (c_2(B-V)+1) + R_1 r(R_2 r+1) + k_c X(B-V). \tag{4.2}$$

It is possible we still might be neglecting some aspects that would improve our results and we might figure them out in the future. For the time being, equation 4.2 is our best model for fitting observed data[3] [34, 24].

---

[2]This correction is also related to spectral difference between used UBVR Johnson filters and used catalog. See more about this issue in following chapter.

[3]This FRAM atmospheric analysis can be only done for cloudless nights which is standard for Observatory sites but rather rare state for Prague, where the prototype is located.

4.2 Hardware and software

Three identical FRAMs are planned for CTA observatory. One prototype was set up in Prague last year for testing purposes. It is based on FRAM from Pierre Auger Observatory, which was successfully operational for a decade. The leading part of FRAM device is 12-inch Schmidt-Cassegrain telescope with Zeiss 135/2.0 photographic lens. It has a narrow-field Moravian Instruments G4-16000 CCD camera. The CCD camera is very sensitive and this combination covers 15×15 degrees FoV. Camera has BVRI Johnson-Bessel filters and a focuser. The whole unit operates on a robotic equatorial Paramount MYT mount. An integral part is housing with a movable roof to provide shelter for the unit and its accessories. The roof can be opened and closed using a hydraulic system with electric valves. The entire setup is completely autonomous.

The whole system operates on RTS2 software developed by Petr Kubánek. This complex open-source package is currently used for dozens of telescopes all over the world. This system runs on Linux and it allows us to control mount, mirrors, cameras and program tasks and simply manage the whole instrument.

FRAM is completely self-operating and autonomous. It turns on a preset time, it opens its dome roof and starts the observing sequence. It is equipped with weather station so it is able to close and shut down in case of a strong wind or rain. It selects the target order according to a predefined queue and it alternates between two scan types. It takes scans in blue filter in order to measure VAOD and in different color filters B, V, R, to obtain Ångström coefficient [34], [36, chapter 5.11].

4.3 Shoot-the-Shower

Program Shoot-the-Shower (StS) was designed for Pierre Auger Observatory. It is used in case some interesting air shower appears on the sky and we want to know the atmospheric condition immediately. This technique is supposed to be quick and efficient. It uses wide-field camera[4] and takes one 30 second scan per minute.

Showers are interesting either because of their high energy which indicates candidates for VHE photons or because of their unusual longitudinal profile. If longitudinal profile shows two maxims (so called double-bump structure) it may point an exotic processes and their observation may provide limits for hadronic interaction models. At the same time, double-bump structure may be caused by aerosol layers or other atmospheric fluctuations. This proves the importance of rapid atmospheric monitoring program. LIDARs can provide very accurate information but their invasive nature does not make them completely fit for this task since their usage means few minutes of downtime for the Observatory. There are no such limitations for FRAM and therefore more showers may be investigated this way. On the other hand, unlike LIDAR, FRAM cannot provide any details about altitude of clouds.

---

[4]FRAM at Pierre Auger Observatory had two cameras, one wide-field and one narrow-field.

4.4 Maps of extinction

Creating so called maps of extinction is the ultimate goal of FRAM observations.

After image taking, it is time for image processing. The first task is pairing observed stars with the Tycho2 catalog [23] and then apply equation 4.2. For each detected light source brighter than 9.5 mag, a corresponding star is found. In order to make this process easier, we split the image into series of sub-images. Whereas the image is affected by vignetting, flat field correction is necessary[5]. Figure 4.2 shows image of identified stars from FRAM prototype.
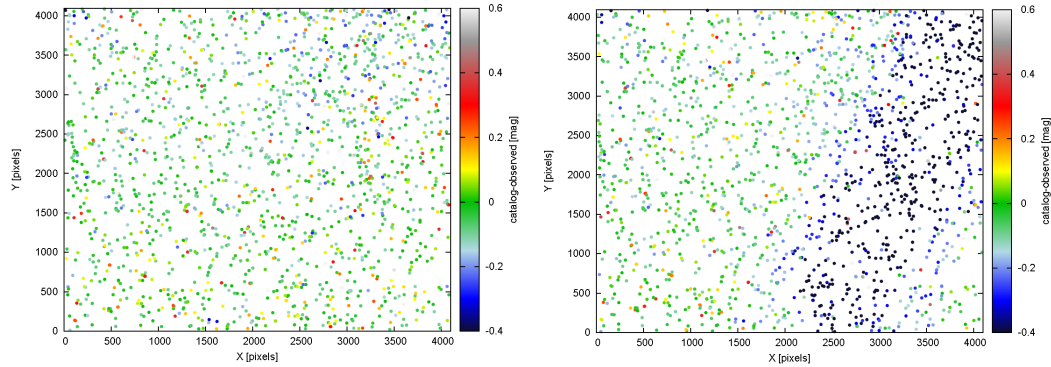
Figure 4.2: Identified stars from image which has been taken by FRAM prototype during clear night in June 2015. Colors show the difference between measured and catalog brightness. In the left figure we can see case of clear sky and in the right figure image with "artificial cloud" created for testing, which caused clear brightness decline. Source: [16].
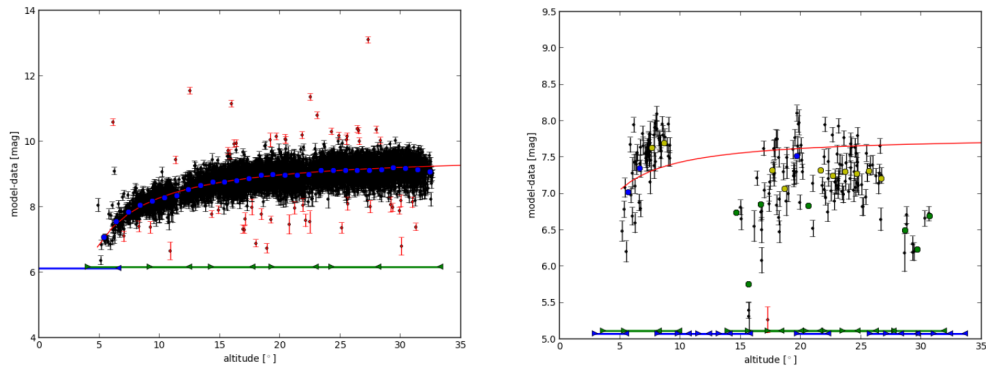
Figure 4.3: Altitude scans for clear sky (left) and cloudy sky (right). Source: [3].

After applying equation 4.2, we judge the outcome in form of so called altitude scans, see 4.3. In the case of clear sky, we can see nicely distributed data where all points sit near the red fitting line. In the case of clouds intervening the observation, we see scattered points further from the red line and at the same time, we see less of them or do not see them at all. As was mentioned above, we can only proceed with our analysis for clear sky images. In order to continue, we

---

[5]We have to be aware of some precision loss in affected areas.

have to go through all altitude scans and manually choose those which are fit for further analysis.

The key quantity for our maps of extinction is VAOD, which we determine by formula 3.3. We are able to do so from a single image. Stars in the image have to be divided into bins. Since star density varies across the sky, adaptive algorithm, which will uniformly bin them, is needed[6]. An example of completed maps of extinction is in figure 4.4. These maps illustratively demonstrate atmospheric conditions above FRAM. They may serve us as a guide during observation at Observatory or we can use them later for the calibration of already measured data.
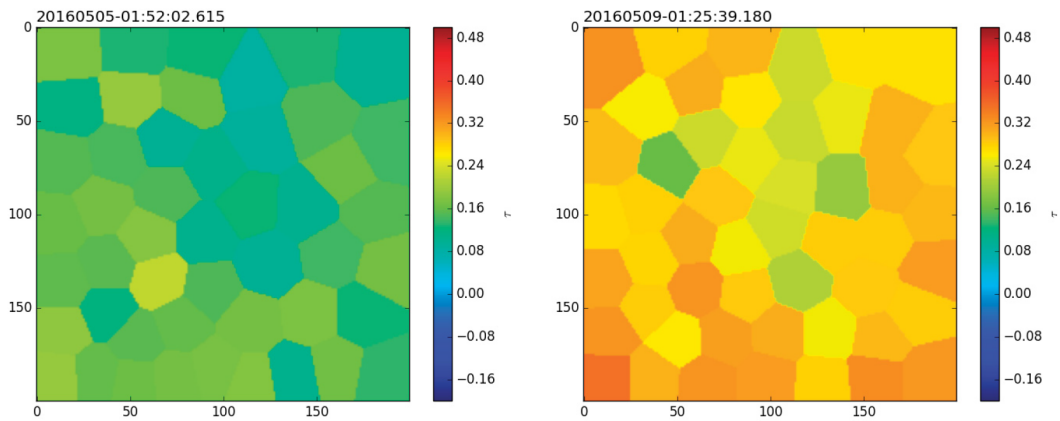
Figure 4.4: Maps of extinction in FRAMs FoV. Colors show varying atmospheric conditions. Source: [16].

---

[6]Voronoi relaxation algorithm has been chosen for this tessellation

5. Data analysis

The FRAM telescope is meant to measure atmospheric conditions at both CTA sites. It has about a decade of working experience from Pierre Auger Observatory in Argentina, but this FRAM was built for a slightly different purpose[1] and therefore its hardware setup is a bit different. So, it needs to be properly tested before departure for CTA sites and also because it is still evolving. FRAM team is constantly trying to improve its function, to develop better model for data fitting, to improve error determination and overall function.

New FRAM prototype 5.1 has been set up in Prague on premises of the Institute of Physics of the Czech Academy of Sciences last spring as was mentioned in previous chapter. It was operational from February 2016 to April 2017. During this time, it has been thoroughly tested and full functionality of the system has been proven. It always worked during clear nights. It was mostly set in its regular observation mode with preset list of targets. It alternately switches between scanning in B filter to get extinction coefficient and ultimately VAOD and between color filters to measure Ångström coefficient.
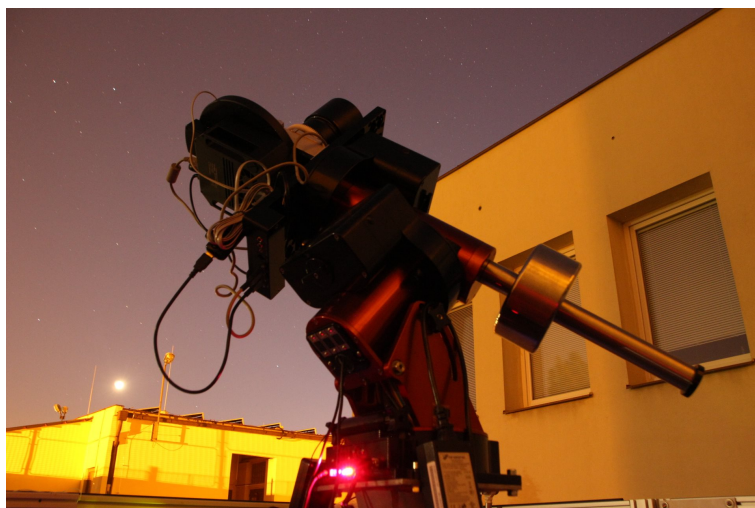
Figure 5.1: FRAM prototype at the Institute of Physics of the Czech Academy of Sciences in Prague. Source: Archive of the Institute of Physics of the Czech Academy of Sciences.

It has taken almost 20 thousands images during dozens of observing nights. A little over thousand from this amount of data is usable for VAOD calculation. Great loss of data is mainly caused by climate and atmospheric condition in Prague. Astronomical sites are carefully chosen locations with little rainfall, low humidity, high amount of clear sky or low cloudiness and it is clear that the center of Prague would never qualify for such purpose. Astronomical sites are also selected at a great distance from big cities, because the influence of people and buildings is harmful for precise measurement. All the disturbing phenomena which astronomers want to avoid, is present at Prague, including light pollution, water vapor and others. Regardless of data losses it is still useful to analyze

---

[1]It does not create maps of extinction and is more used for rapid monitoring program instead.

remaining data. And even though we expect higher VAOD values, we may later use this data for comparison and confrontation with newly collected data at CTA sites.

5.1 Data modeling

All images which have been taken during the observation have been analyzed by the following pattern. As was said in previous chapter, FRAM uses CCD chip to record signal. Incoming flux of photons is thus converted to electrons and further transformed to a measurable electric signal. There are always uncertainties associated with electronic instruments like noise or dark current. Effect of the noise is mostly eliminated for the most of the pixels if the chip is cooled down to $-20\,°\mathrm{C}$. For our measurement only temperature below $-19\,°\mathrm{C}$ has been accepted, any other temperature has been excluded from further analysis. The elimination of dark current is done by subtracting so called "dark frame". The telescope takes some images with closed shutter, which are later summed up and their mean value is used for the subtraction[2]. Another issue is the correction of vignetting and imperfections. This is done by creating series of uniformly lit images, which will later create so called "flat field", by which we divide existing value. This way, the removal of all possible defects of optics or electronics or presence of dust or dirt, which causes (on average) same disruption of each frame, is ensured. It is a standard procedure used by astronomers all over the world.

Next step in the analysis is aperture photometry. Every single light source representing a star is taken and two concentric circles are drawn around it, according to figure 5.2. Firstly, all detected light is summed up in the inner circle, secondly, values from larger circle are taken for background determination and are later subtracted from the first value.
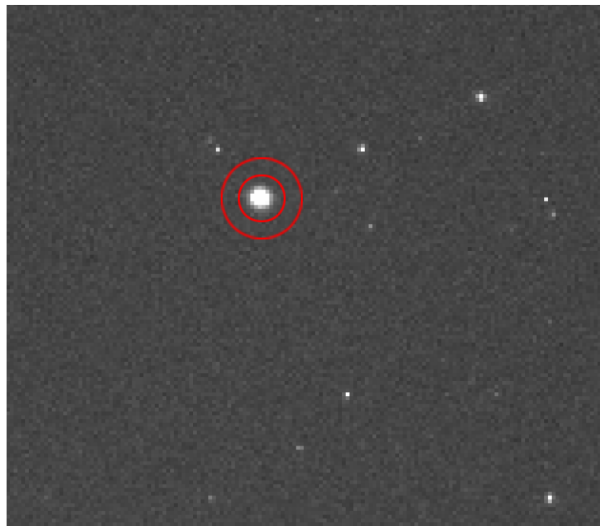
Figure 5.2: Illustration of aperture photometry principle. Source:[19].

In this stage star detection algorithm is due. Only stars with magnitudes

---

[2]Even after using this procedure, there are some deviations caused by small temperature changes during the night. This effect is small and our group works on a better solution [19].

higher than 6.5 mag and lower than 9.5 mag have been chosen for this detection. Pairing weaker light sources with catalog is not reliable and stronger sources are over-saturated and therefore usage of either of them is not desirable. Another restriction concerns airmass. As explained before, airmass for observing zenith angle Θ_Z equals to one, see 5.3. However, if we observe the sky under different angle, we also observe it trough different amount of airmass. More specifically, it is approximately inversely proportional to $\cos\Theta_Z$[3]. It was decided from experience that $X = 4.5$ should be the limit for conditions in Prague, because it is difficult to identify stars lower on horizon due to pollution of the atmosphere and also limited view. Even with this value, we can find images with pieces of trees or buildings, which block the FoV and do not allow full size analysis. In previous chapters we shortly mentioned influence of different wavelengths or colors of incoming star light. Here we have to consider spectral difference between used UBVRI Johnson filters and values of colors in Tycho2 catalog[23], which we use for identification[19]. According to the previous research, B filter used by FRAM is shifted towards longer wavelengths and therefore has to be calculated by adding up $0.7B_{Tycho}$ and $0.3V_{Tycho}$. At the same time, it is only applicable for stars that meet formula $0.7B_{Tycho} - 0.3V_{Tycho} < 0.8$ due to two apparent observed star populations, see [19].
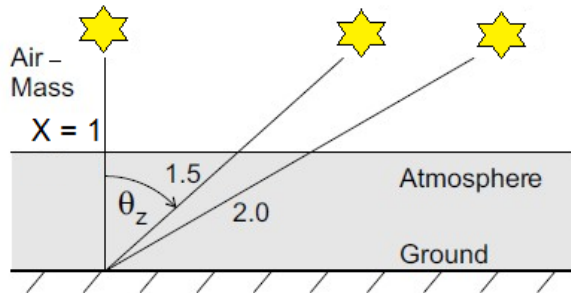
Figure 5.3: Airmass illustration. It equals 1 for the zenith observation and it increases with the zenith angle Θ_Z. Source: [35], altered.

In order to avoid distortion, we divide the image into tiles. After severe testing, configuration with 4×4 tiles where 4 central tiles are merged into one big tile has been selected. After that, we apply equation 4.2[4] to every tile and we proceed to data fitting. Many other configurations have been tried, see figure 5.4 for comparison of 3×3 configuration with the chosen one. It is clear that at the right diagram there are smaller deviations and smaller vignetting effect in individual segments.

It is only possible to measure VAOD for clear nights, as explained in previous chapter, so manual data selection is in order. We went through all altitude scans and excluded all those which were not suitable for analysis by dismissing scans significantly deviating from an ideal featureless extinction profile.

After we fit the data with our model 4.2, we are able to obtain extinction coefficient k. This equation was used instead of simply using the original one 3.1

---

[3]For more detailed determination see [19]

[4]See previous chapter for explanation of this equation.
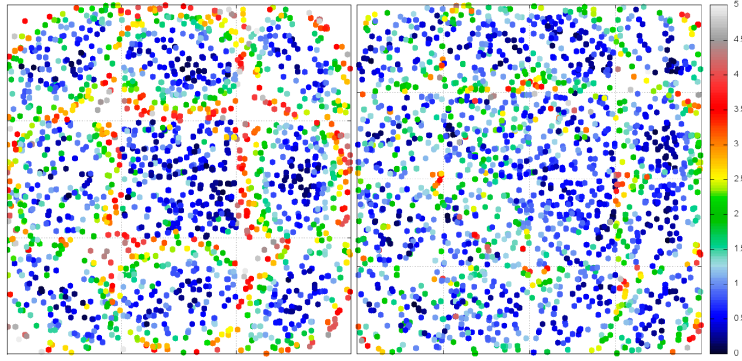
Figure 5.4: Colored points in this figure show the difference between detected light sources and positions of stars in Tycho2 catalog in pixels. Left diagram shows splitting original picture into 3×3 tiles and right diagram shows 4×4 splitting with bigger inner tile merged from 2×2 tiles, which is now used configuration. Source: [19].

or 4.1, from which this equation was derived. In the same manner, we will replace it in equation 3.3 and we will get

$$\text{VAOD} = 0.921 \cdot k - \tau_{\text{Ray}}. \tag{5.1}$$

Therefore, the only thing remaining for VAOD calculation is to determine τ_{Ray}, which stands for molecular contribution. In the case of monitoring in blue light, this effect is dominated by Rayleigh scattering. The value τ_{Ray} has been found analogously to article [19], which is based on [4]. For crude estimation, we firstly calculate Rayleigh attenuation length according to [15]

$$\Lambda = 2974 \cdot \left(\frac{\lambda}{400 \text{ nm}}\right)^4 \text{ g} \cdot \text{cm}^2, \tag{5.2}$$

for filter effective wavelength $\lambda = 435$ nm. And secondly, Rayleigh scattering itself

$$\tau_{\text{Ray}} = \frac{p_{\text{P}}}{100 \cdot \Lambda}, \tag{5.3}$$

where p_{P} stands for atmospheric pressure in Prague, which is about 350 m above see level. This way, we can estimate the contribution of Rayleigh scattering for 0.23.

For estimation of the exact value, we need to consider more factors. Firstly, we need to know the spectrum of incoming light. It is possible to use cataloged spectra for great number of stars and then fit this measured data and use the fitted mean spectrum for the calculation. This turned out to be the most accurate way[5], once again at least for stars which obey $B-V < 1$. Next we need to consider spectral response of the whole FRAM unit. This consist of transmission of used B filter, transmission of optical system and also spectral response of the electronics. The overall spectral response of the combined system has to be convoluted with the wavelength dependency of Rayleigh scattering. After extensive measurements and calculations, the value has been determined and it equals to 0.212.

---

[5]Another way would be to consider every star to be black-body radiator of given temperature.

5.2 Uncertainty estimation

The integral part of every measured value in every field is its uncertainty or error range. To estimate the precision of our VAOD values, we have to consider a great deal of effects and processes. To overall uncertainty both statistical and systematic uncertainty contribute.

The calculation of statistical uncertainty has to start with the accuracy estimation of a single star. From a single star to a single image and from a single image to series of seven images, which usually forms a single observation scan. For each of these scans, we know the value of extinction coefficient k together with its statistical uncertainty. At the following figure, you can see histogram from all measured data, which is 1113 images.
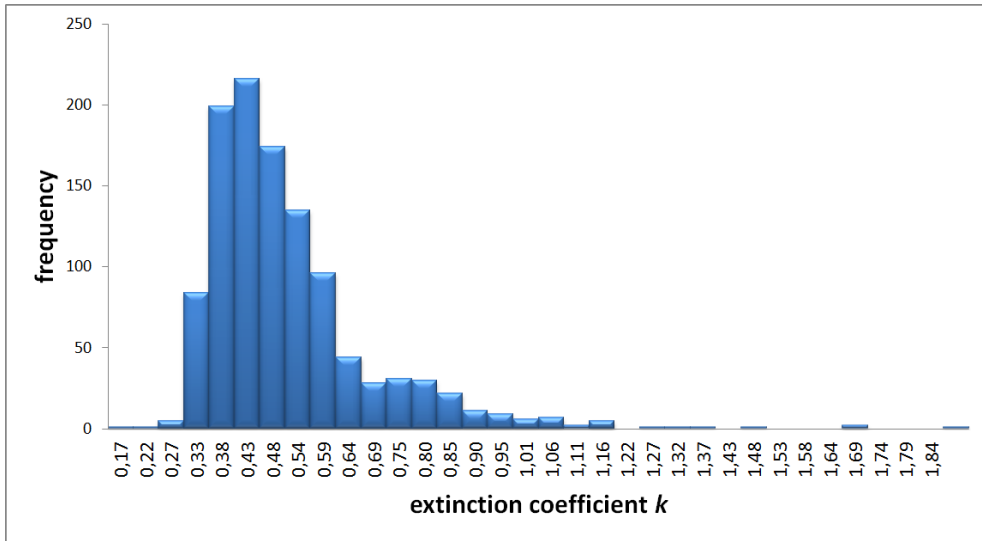
Figure 5.5: Histogram of obtained extinction coefficient k values. The mean value is 0.47 ± 0.09 and median is 0.45. We can see that our set of values has approximately Poisson distribution.

Uncertainty in measurement of a single star is given by the sum of uncertainty done by estimation of its apparent flux J and magnitude uncertainty indicated by Tycho2 catalog which equals to 0.1 mag:

$$\sigma_{\text{star}}^2 = \sigma_{\text{J}}^2 + \sigma_{\text{M}}^2. \tag{5.4}$$

Error of the determination of the coefficient k is then estimated by calculating the RMS over the whole image, using the usual prescription

$$\text{RMS}^2 = \frac{1}{n} \sum_n \frac{(m_{\text{obs}} - m_{\text{fit}})^2}{\sigma_{\text{star}}^2}, \tag{5.5}$$

where the numerator is the difference of squares of observed and fitted magnitude and n is the number of stars in the image. For every k, we calculated its statistical uncertainty and then we made histogram from those values, see 5.6. We confirmed that these uncertainties should be less than 0.01, which is the value estimated at [19].

Those uncertainty values are small compared to the systematic uncertainty.
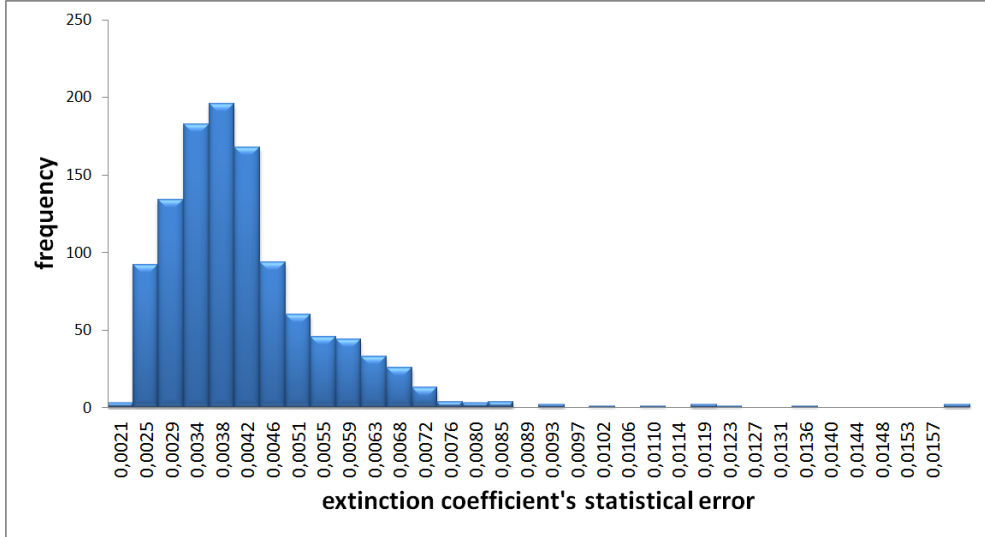
Figure 5.6: Histogram of obtained uncertainties of extinction coefficient k.

The systematic uncertainty is dominated by the uncertainty created by Rayleigh subtraction. This uncertainty has been estimated in [19] and it approximately equals to 0.02. This number is by itself larger than statistical uncertainty and it corresponds only to a possibly imperfect laboratory measurement of the optical system, ignoring other sources of systematic uncertainties. For example, the Rayleigh subtraction value also varies with temperature and therefore the time of observation. However those changes are in order of thousandths or hundredths, which we neglected for this purpose.

Another systematic shift may be caused by uniformly distributed layer of aerosol in the atmosphere which will dim all the light sources in the same way and FRAM will not be able to identify this issue, since it only measures relative apparent light flux and does not have absolute scale for comparison.

There may be other sources of systematic uncertainty which we are yet to discover.

Combination of statistical uncertainty and estimated systematic uncertainty is entirely sufficient for measurements in Prague, but for conditions at CTA sites further analysis of systematic uncertainties is needed.

5.3   VAOD analysis

We calculated VAOD using every extinction coefficient k which was determined from every satisfactory observing image. From all these VAOD values, we assembled histogram 5.7.

Similar measurements have been carried out at Pierre Auger Observatory in the past. VAOD values there are normally lower than 0.1 because there are nearly perfect atmospheric conditions for astronomic observations. We expected higher values for Prague, whereas the local conditions are much worse, as was mentioned above. As we can see from histogram 5.7, typical value for Prague is around 0.2. This means that our measurements results are in line with the theory.

There are some individual results which stood out because of their extreme
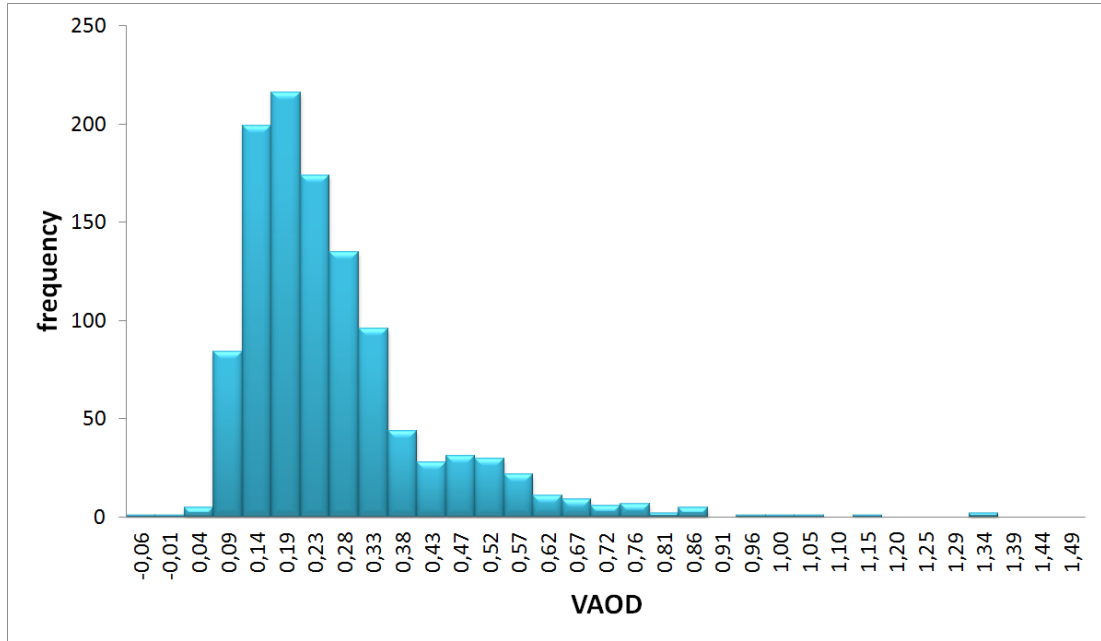
Figure 5.7: Histogram of obtained VAOD values. The mean value is 0.24 ± 0.17 and median is 0.20. We can see that our set of values has approximately Poisson distribution. For the estimation of mean VAOD value of every observing night, see Attachment B.

value. For example, we have two negative values and several values which are too high (e.g. higher than 0.9) even for local conditions and should be checked.

5.3.1 Discussion of measured values

Our interest is the VOAD development depending on time. Time of the image taking is always a part of every data file so we can plot this dependency for every observing night through the whole measuring period in Prague. We divided this period by moths and created plot for one of them. At figure 5.8 we have this plot for January. All other observing nights are plotted in the same way at figures in Attachment A divided into the appropriate months. Longer breaks between observing nights have been caused by technical work on FRAM unit.

In the winter, there are long nights and short days in the Czech Republic. That means there is more time for astronomic observations. At the figure 5.8, we can see that it was possible to scan the sky approximately from 6 p. m. to 6 a. m.[6].

Typical examples

We can see that the observing night from January 10 to January 11 was very successful. We examine it closer at figure 5.9. We have a lot of data in range from 0.18 to 0.28, all spread near 0.2 which is a typical value as we know from histogram 5.7. We assume they were taken during a clear night and we can

---

[6]This and all following times are for the CET (Central European Time) zone.
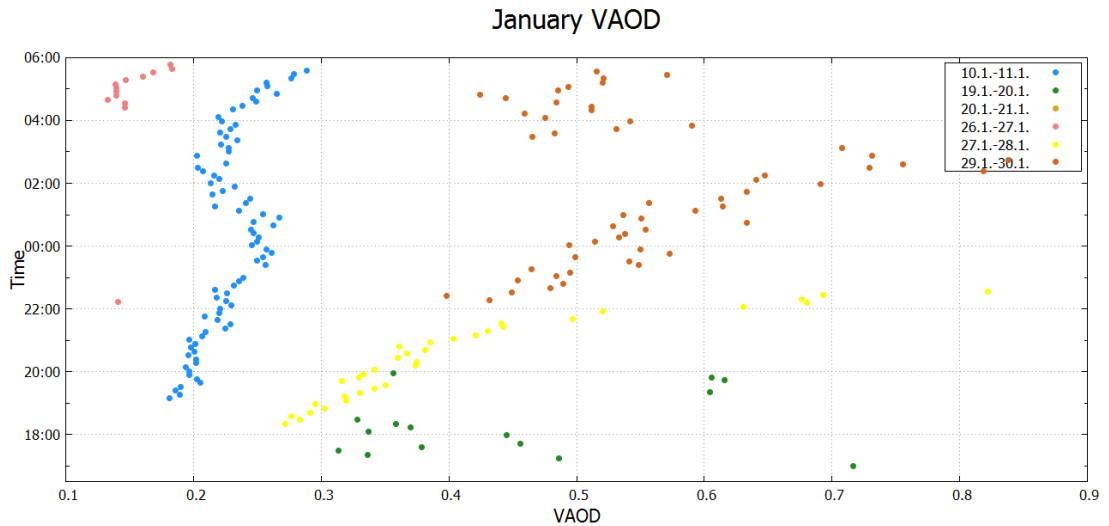
Figure 5.8: Calculated VAOD for data observed in January 2017.

verify that by confronting it with the weather data. We looked up data related to cloudiness at the Internet[7] and confirmed clear sky from 7 p. m. to midnight and arrival of high cloud layer in morning hours.
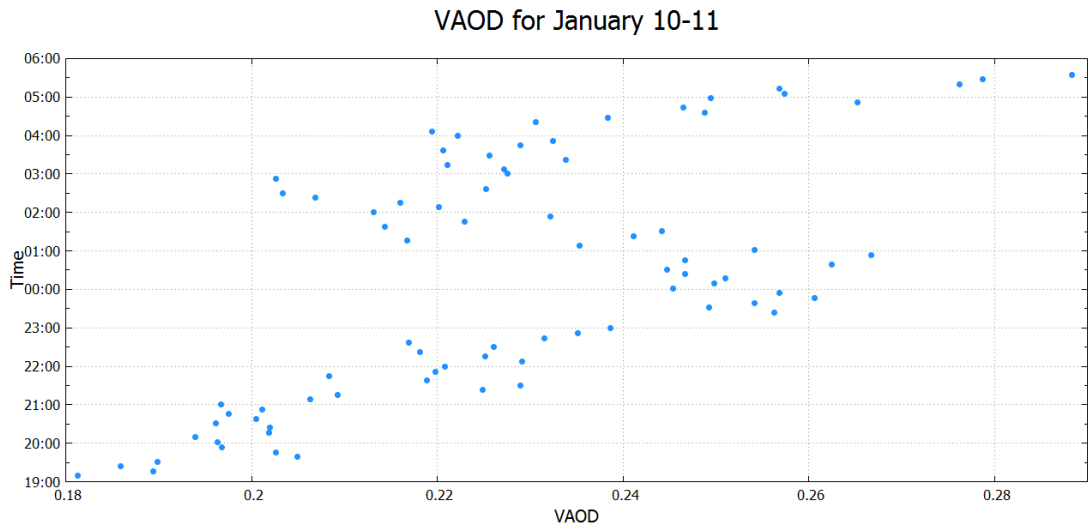
Figure 5.9: Calculated VAOD for data observed on the night from January 10 to 11.

It is possible to find image from approximately same time as the radar image at the left side of figure 5.10 to show an example of a "nice" image. We can see this image at 5.11. Lot of stars are clearly visible in this image which means photometry can run properly and we get reasonable VAOD values at the end of the process. On the right side of figure 5.10, we can see Prague under the layer of hight clouds, which by itself doe not necessarily mean the measurement cannot

---

[7]All radar images in this chapter have been taken from the on-line weather site http://aktual.meteopress.cz/oblacnost.php.
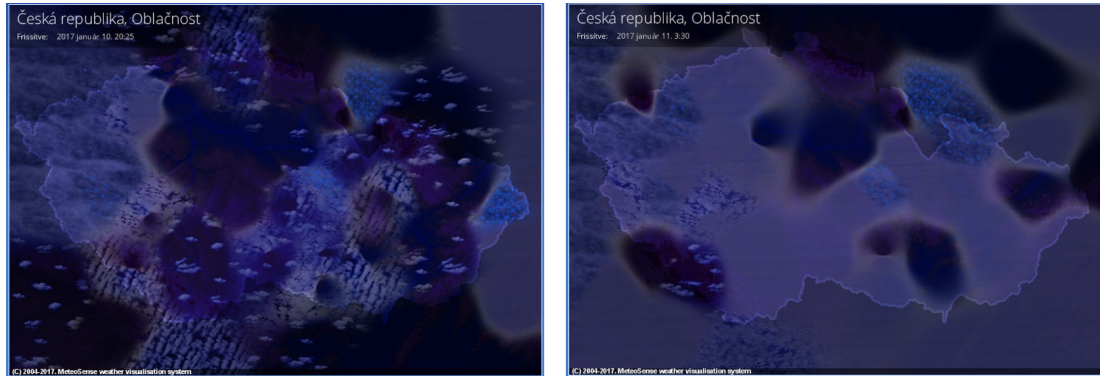
Figure 5.10: Cloudiness on the night from January 10 to 11. Dark places represent the absence of any kind of clouds. We can see clear sky above Prague in the left picture from 20:25 and layer of high clouds in the picture on the right from 3:30.
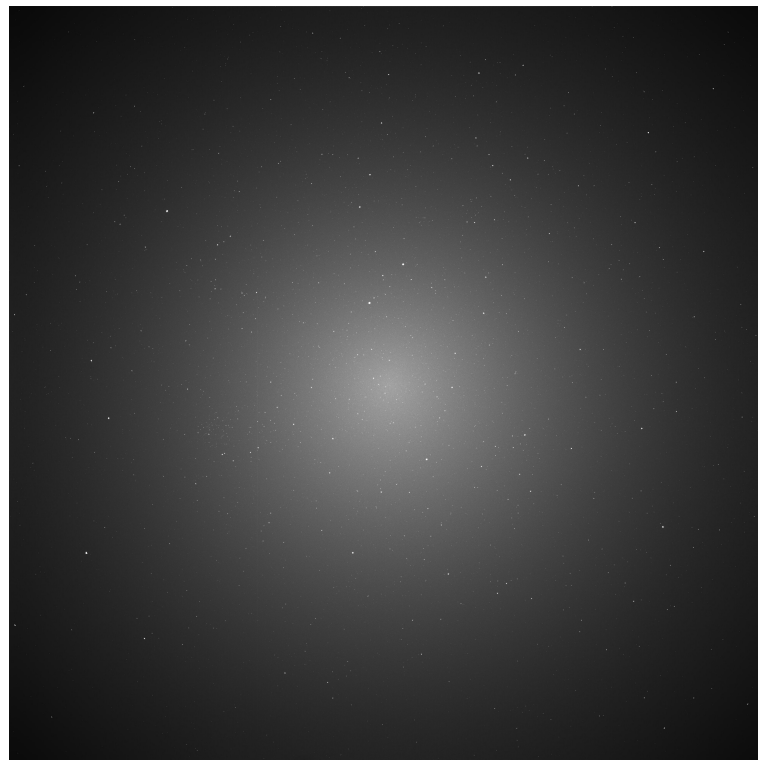
Figure 5.11: Raw image taken by FRAM on January 10 at 20:28. We can see a star field typical for Prague. There is also considerable vignetting at the picture, because image was not corrected for dark and flat field yet.

be successful. We see at figure 5.8 or 5.9 that VAOD values are little higher but still consistent with the rest of the night.

Lets take a look at another observing night, for instance January 26 - 27. We see that there is very little data but we have very good values at the end of the night. At figure 5.12, we can see the course of the night. At the top left image there is very cloudy sky and that is why we do not have any data available. After that, sky cleared a little and only low clouds endured and short series of measurement has been taken. However, only one image was suitable enough for

processing. Low cloudiness persisted to the morning hours and sky completely cleared after 4 a. m. when FRAM took another data series.

Very illustrative night is from November 10 to 11, you can si VAOD data from this night at figure 5.13. Data are very consistent (and less than 0.1) for the first part of the night and after 22:00 o'clock they spread up to 0.9. Once again, this indicates cloud arrival.
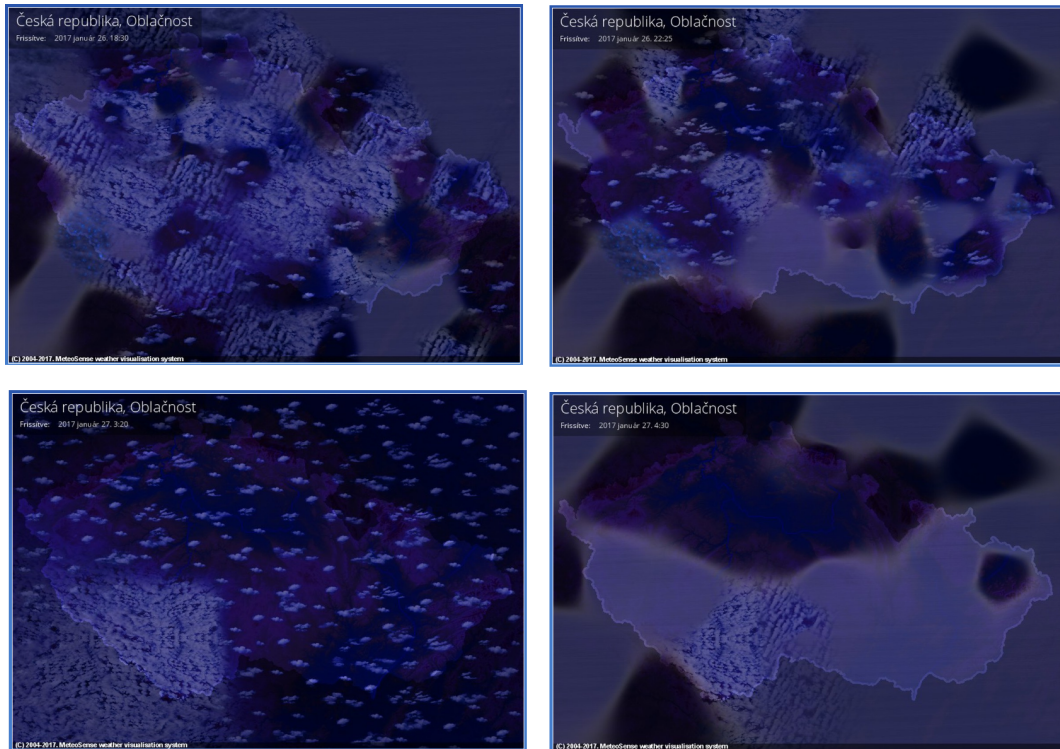
Figure 5.12: Cloudiness on the night from January 26 to 27. Dark places represent absence of any kind of clouds.
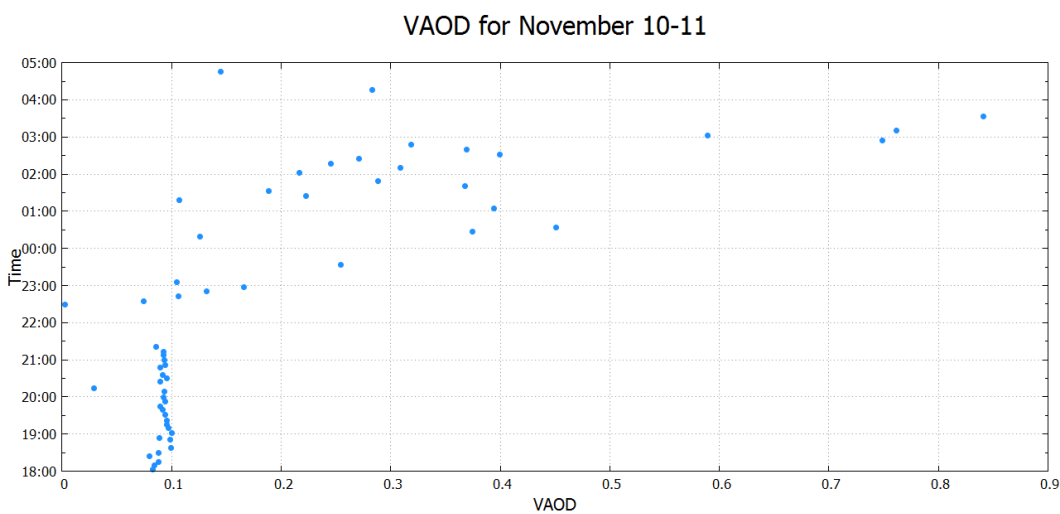
Figure 5.13: Calculated VAOD for data observed on the night from November 10 to 11.

Firstly, let us look at one picture from the first part of the night where sky

should be clear. We can confirm this assumption by looking at figure 5.14. There we have FRAM's raw image of a clear sky and at the right state of the weather, where clouds do not appear to be directly above our measuring station.

Around 23:00 o'clock, conditions worsen abruptly. As we can see on the left side of figure 5.15, some images were disturbed by the presence of clouds, which is indicated by streaks of light which is visibly shifted. Radar image on the right side confirms that at this time both high and low clouds were present. Nevertheless, some images have not been dismissed and that is why we have some data at figure 5.13 with much higher value than before.
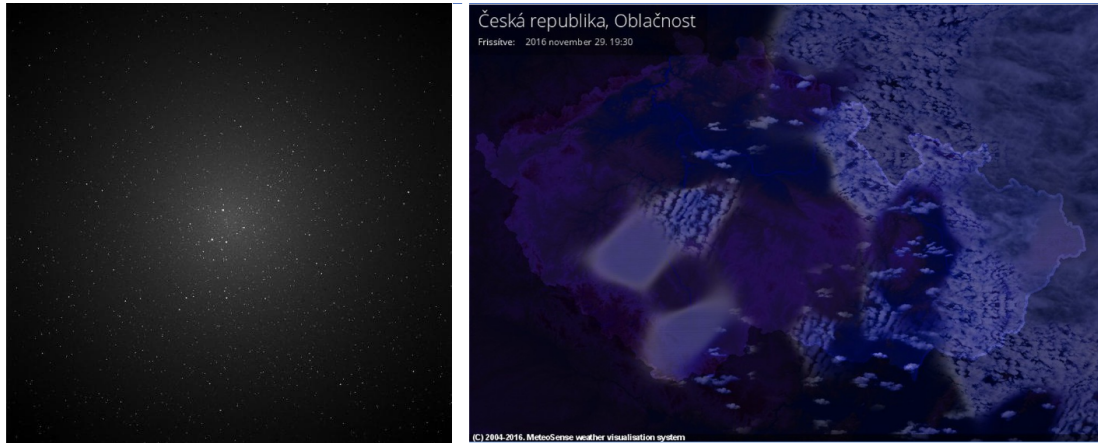
Figure 5.14: Raw image taken by FRAM on November 10 at 19:21 on the left. Cloud conditions approximately at the same time (19:30) on the right.

Figure 5.15: Raw image taken by FRAM on November 10 at 23:30 on the left. Cloud conditions approximately at the same time (23:20) on the right.

The rest of the second part of the night proceeded in a similar way. The sky was cloudy and therefore VAOD values were higher. At figure 5.16, we can see analogical course to previous example 5.15.

We do not have any data after 5:00 o'clock, because conditions worsen so much it was no longer possible to pick up any successful image. Even so, we can

Figure 5.16: Raw image taken by FRAM on November 10 at 3:56 on the left. Cloud conditions approximately at the same time (3:20) on the right.

Figure 5.17: Raw image taken by FRAM on November 10 at 5:31 on the left. Cloud conditions approximately at the same time (5:25) on the right.

find some blurred images, similar to the one at figure 5.17. The image is deformed by clouds so much we cannot see almost any stars and therefore is not possible to analyze it further.

We can say our predictions agree with the reality and our VAOD measurements correspond with the state of the weather.

One point (around 20:00) at figure 5.13 significantly deviates from the rest of the data from the first part of the night. Its value is suspiciously low and requires our attention. Relevant image is on the left at figure 5.18, together with zoomed in detail on the right. It is clear that a part of some building (upside down) is in the way of FRAM's FoV. It does not necessarily have to be a problem, because we see clear sky on the rest of the image and that can be enough for the star detection algorithm. We also see that this building interferes with more than one tile. The most problematic parts are probably the antennas or thin objects on the roof, which considerably deform incoming light which seemingly shines through them. It is a good thing we can spot this without going through all
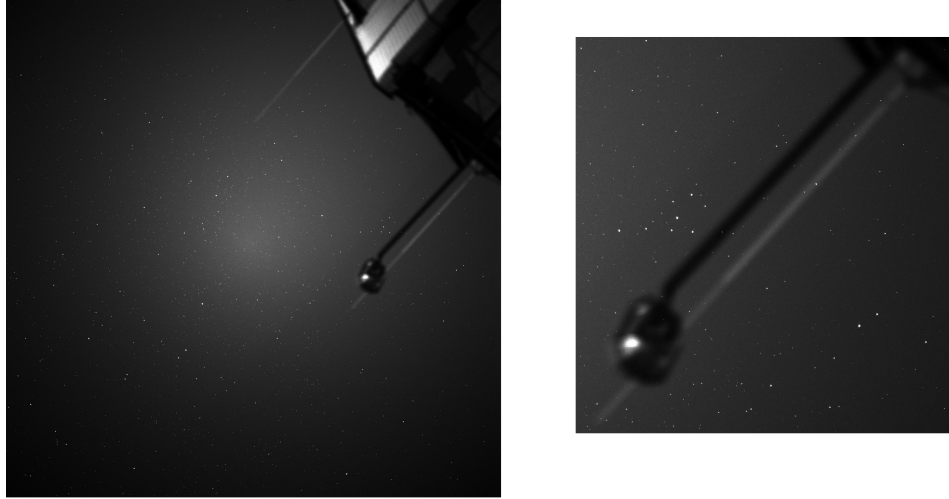
Figure 5.18: Raw image taken by FRAM on November 29 at 20:14 on the left. Cut out detail of antennas at the top of the building on the right.

images manually, but this kind of issue is not something we will deal with at CTA sites, where the FoV is clear.

We could analyze every night in the same manner. However the pattern seems to be clear and we are confident we can rely on these measurements. Surely there can be found some other interesting nights, see Attachment A. However, examples above have been handpicked to illustrate and characterize behavior of this VAOD measurement which should be valid for all of them.

5.3.2   Treatment of anomalies

As was mentioned above, we have to take a look at some extreme values, because they represent some kind of anomaly. Values which are out of ordinary are negative ones together with suspiciously low ones. And from the other part of spectrum, values which are too high.

Negative values

On figure 5.19 we see the lowest measured value, which is negative. Considerable part of the image is shaded by a tall tree, part of the building and a fence. On figure 5.20, there is a detail of the tree and the situation is similar to the one on figure 5.18, stars shine through a tree and we cannot rely on such light sources. Analogically to the previous situation, the VAOD value is lower than it is supposed to be. When we take a look on the altitude scan on the right side of figure 5.20, we see that the decrease of values was too fast and thus these data were not included into the analysis of this particular scan, which led to faulty course of fitting curve and ultimately to the wrong calculation of its slope, that is extinction coefficient k. After this analysis, we can conclude that this altitude scan should have been dismissed during selection. The second negative value has been calculated from image which has been taken from the same angle as the one on figure 5.20 and the explanation goes the same way.

Figure 5.19: Raw image taken by FRAM on February 2 at 21:33. This image led to calculation of negative VAOD value.
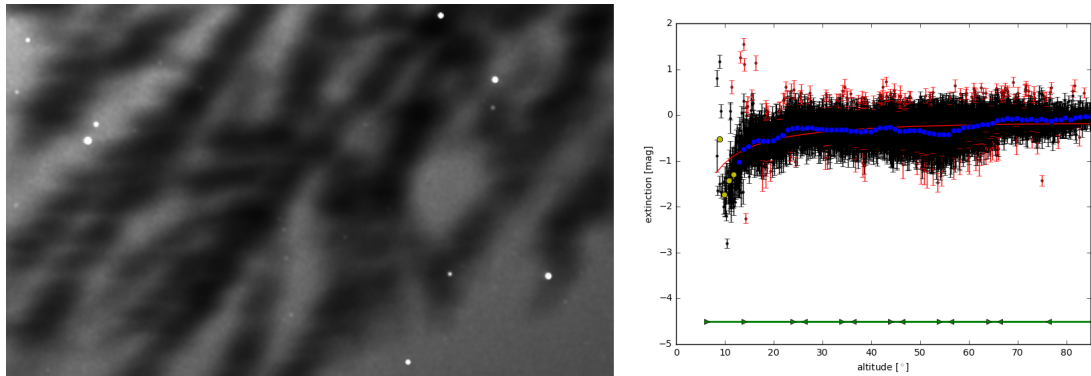
Figure 5.20: Data related to image taken on February 2 at 21:33 which resulted with negative VAOD value. On the left side detail of the tree from figure 5.19 and on the right side altitude scan of the same measurement.

Abnormally high values

Altitude scans for very high VAOD values are at figure 5.21. They are all from the same series of measurements, night from May 21 to 22, see 5.25. All these dependencies drop too soon and the fitting curve does not get the right shape. When we examine image of one of them at figure 5.22, we see that the sky was extremely cloudy and FRAM could not see almost any stars. This is only confirmed by radar image on the right side of the figure 5.22. It makes sense for those values to be out of chart, since photometry could not run properly. Thus we see that the shape of altitude scans, similar to those at figure 5.21, is also reason for the image exclusion and we should have dismissed them during selection.

Once again, this is not something CTA will have to deal with because as was mentioned, at CTA sites additional weather data from other calibration in-

struments will be available. There will be all sky cameras, photometers and ceilometers and other instruments which will monitor other atmospheric parameters and we will be able to use them to identify situations which lead to these kind of extreme data.
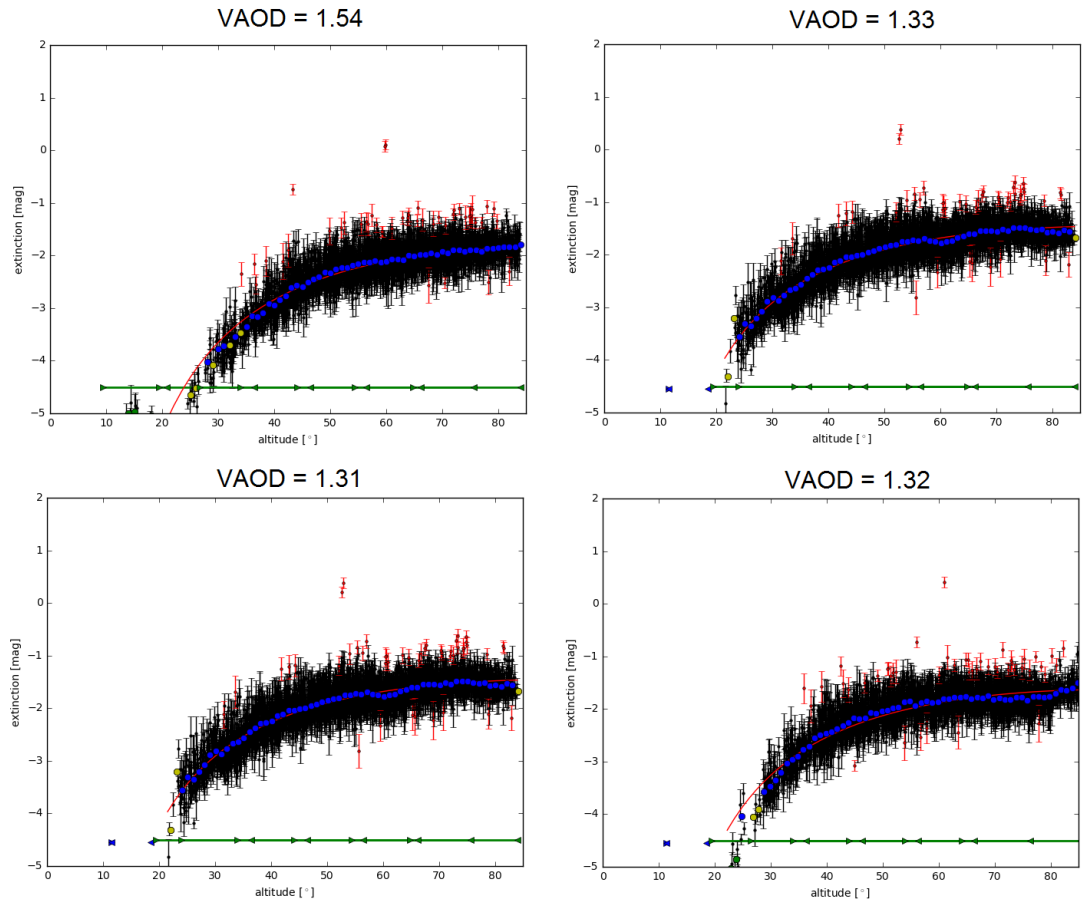
Figure 5.21: Altitude scans of measurements with abnormally high VAOD value.
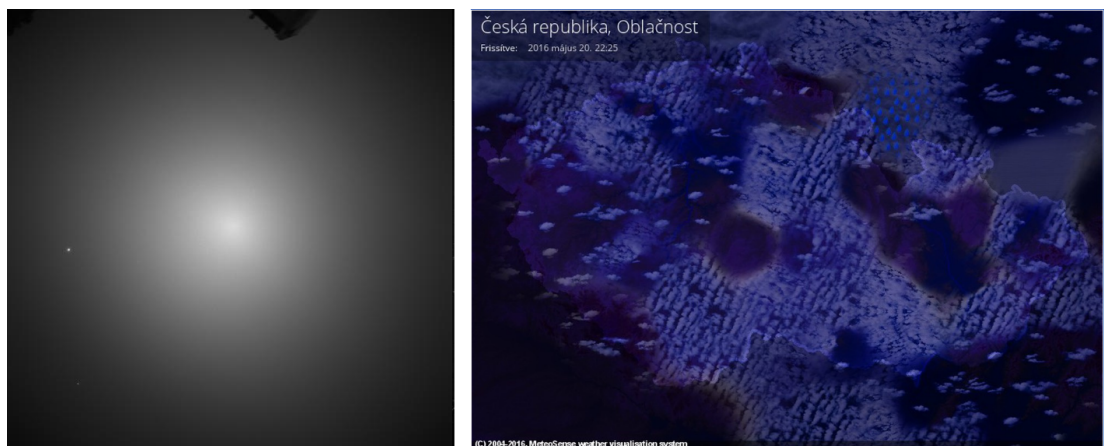
Figure 5.22: Raw image taken by FRAM on May 21 at 22:09 on the left. Cloud conditions approximately at the same time (22:25) on the right.

5.4 Measurement of Ångström coefficient

In equation 3.2 we defined Ångström exponent and we already mentioned FRAM can perform measurements with color filters to obtain this coefficient.

This measurement together with its analysis is more complicated than VAOD measurement. It needs to be more precise because within the analysis we need to evaluate the difference of two numbers, measured value and estimated molecular part of optical depth, and the numerical values of these parts are very similar for measurements in other filters than in B. It is therefore very important to minimize all systematic uncertainties.

For example, the presence of the Moon, especially around full moon, creates an extra background with strong gradient which is difficult to correctly remove and thus it is complicated to obtain the precise photometry for individual stars. The typical result is that with improper treatment of the Moon we often obtain negative values of VAOD.

Values of Ångström coefficient usually range from 0 to 2. We get lower values for coarse particles and desert dust, higher values for fine particles and automobile exhaust.

This analysis have not been done for the data measured by FRAM prototype in Prague yet. It will be part of our future work. We expect Ångström coefficient to vary there between 1.5 and 2, because the fine grain particles from automobile exhaust dominate in such an environment of a big city.

Conclusion

FRAM telescope prototype has been successfully installed in Prague and performed dozens of observing nights through the course of fourteen months. During this time, it took almost 20 thousand images which where further analyzes by star detection algorithm and modeled using fitting parameters.

CCD chip has been cooled down below $-19\,°\mathrm{C}$ to eliminate the dark current. Every image has to be corrected on flat and dark field. After these steps, algorithm detects every light source and subtracts its background. Then, it identifies every source between 6.5 and 9.5 mag and finds corresponding stars at the Tycho2 catalog in separate predefined tiles.

Acquired data are then fitted using equation which has been developed for this purpose and it is described in detail in chapter 4. There are many factors which need to be considered, e.g. the dependence of the optical parameters of the instruments on the environmental conditions or the influence of Rayleigh scattering. The extinction coefficient can be correctly obtained only for clear nights without clouds, therefore we manually checked and dismissed all those images which are influenced by presence of clouds.

Using this procedure, we obtained 1113 VAOD values and we plotted them into histogram. This histogram showed Poisson distribution with mean value 0.24 ± 0.17 and median 0.20. This value is much higher than the one from the Pierre Auger site, where it usually does not overgrow 0.1. Results are therefore in line with the expectations.

Among the results, there were 2 negative values which needed to be examined. We have found that in both cases something has been standing in the field of view and shifted or deformed incoming light. Such measurement is not reliable and ultimately should be excluded from our set of values. We have also found that value is often lower in similar cases of involuntary light shielding.

There were some cases of VAOD value too high even for conditions in Prague. When we looked at the raw images together with radar images of cloudiness we have found there was too many clouds for proper function of star detection algorithm.

We plotted all the observing nights divided by months and we further analyzed some individual nights. We spotted consistent values near 0.2 for clear parts of the nights. The presence of clouds usually shifts VAOD to higher values. VAOD values are also spread across a wider range of values and less reliable.

Through data analysis, we concluded that FRAM's system is fully functional and prepared for measurements at CTA sites.

We will now follow this part of analysis with the analysis of data measured in color filters and the calculation of Ångström coefficient.

Bibliography

[1] Konrad Bernlöhr. Corsika and sim_telarray – simulation of the imaging atmospheric cherenkov technique. Technical report, 2017.

[2] C. Bigongiari. The Cherenkov Telescope Array. *ArXiv e-prints*, June 2016. `arXiv:1606.08190`.

[3] Jiří Blažek. Searching for anomalous profiles with fram. talk at AtmoHEAD Olomouc, 14. 9. 2016.

[4] Anthony Bucholtz. Rayleigh-scattering calculations for the terrestrial atmosphere. *Appl. Opt.*, 34(15):2765–2773, May 1995. URL: `http://ao.osa.org/abstract.cfm?URI=ao-34-15-2765`, `doi:10.1364/AO.34.002765`.

[5] CTA collaboration. Cherenkov telescope array: Exploring the universe at the highest energies. `https://www.cta-observatory.org/`. Online; accessed: 2017-01-08.

[6] CTA collaboration. Cherenkov telescope array: How cta works. `https://www.cta-observatory.org/about/how-cta-works/`. Online; accessed: 2017-01-08.

[7] CTA collaboration. Cherenkov telescope array: Technology. `https://www.cta-observatory.org/project/technology/`. Online; accessed: 2017-01-08.

[8] CTA collaboration. CTA Prototype Telescope, ASTRI, Achieves First Light. `https://www.cta-observatory.org/cta-prototype-telescope-astri-achieves-first-light/`. Online; accessed: 2017-01-08.

[9] CTA collaboration. Flicker: Cherenkov telescope array observatory. `https://www.flickr.com/photos/cta_observatory/`. Online; accessed: 2017-01-08.

[10] CTA collaboration. Common technology evaluation, testing and calibration technical design report. Technical report, CTA Construction Project, 2016.

[11] H.E.S.S. collaboration. High energy stereoscopic system. `https://www.mpi-hd.mpg.de/hfm/HESS/`. Online; accessed: 2017-01-08.

[12] MAGIC collaboration. Major atmospheric gamma imaging cherenkov telescopes. `https://magic.mpp.mpg.de/`. Online; accessed: 2017-01-08.

[13] Veritas collaboration. Very energetic radiation imaging telescope array system. `https://veritas.sao.arizona.edu/`. Online; accessed: 2017-01-08.

[14] J. W. Cronin. The highest-energy cosmic rays. *Nuclear Physics B Proceedings Supplements*, 138:465–491, January 2005. `arXiv:astro-ph/0402487`, `doi:10.1016/j.nuclphysbps.2004.11.107`.

[15] Bruce Dawson. New rayleigh scattering implementation in the offline. *GAP-2006-007*, Jan 2006.

[16] J. Ebr, P. Janecek, M. Prouza, J. Blazek, and f. t. CTA Consortium. Real-time atmospheric monitoring for the Cherenkov Telescope Array using a wide-field optical telescope. *ArXiv e-prints*, August 2015. `arXiv:1508.06798`.

[17] J. Ebr, M. Prouza, M. Jelínek M. Mašek I. Ebrová P. Janeček, P. Kubánek, and J. Černý. Shoot-the-shower: real-time observations for astroparticle physics using the fram robotic telescope. *The Proceedings of the Third AstroRob Workshop (2013)*, 2013.

[18] Jan Ebr. Atmospheric calibration of the cherenkov telescope array. 2017.

[19] Ebr, Jan, Blažek, Jiří, Prouza, Michael, Mandát, Dušan, Pech, Miroslav, Mašek, Martin, Juryšek, Jakub, Janeček, Petr, Kubánek, Petr, Eliášek, Jiří, Jelínek, Martin, and Ebrová, Ivana. Aerosol measurements with the fram telescope. *EPJ Web Conf.*, 144:01011, 2017. URL: `https://doi.org/10.1051/epjconf/201714401011`, `doi:10.1051/epjconf/201714401011`.

[20] B.S. Acharya et al. Introducing the cta concept. *Astroparticle Physics*, 43:3 – 18, 2013. Seeing the High-Energy Universe with the Cherenkov Telescope Array - The Science Explored with the CTA. URL: `http://www.sciencedirect.com/science/article/pii/S0927650513000169`, `doi:http://dx.doi.org/10.1016/j.astropartphys.2013.01.007`.

[21] A.M. Hillas. Evolution of ground-based gamma-ray astronomy from the early days to the cherenkov telescope arrays. *Astroparticle Physics*, 43:19 – 43, 2013. Seeing the High-Energy Universe with the Cherenkov Telescope Array - The Science Explored with the CTA. URL: `http://www.sciencedirect.com/science/article/pii/S0927650512001326`, `doi:http://dx.doi.org/10.1016/j.astropartphys.2012.06.002`.

[22] Jim Hinton, Subir Sarkar, Diego Torres, and Johannes Knapp. A new era in gamma-ray astronomy with the cherenkov telescope array. *Astroparticle Physics*, 43:1 – 2, 2013. Seeing the High-Energy Universe with the Cherenkov Telescope Array - The Science Explored with the {CTA}. URL: `http://www.sciencedirect.com/science/article/pii/S0927650512002198`, `doi:https://doi.org/10.1016/j.astropartphys.2012.12.002`.

[23] Hog E., et al. The Tycho-2 Catalogue of the 2.5 Million Brightest Stars. *Astronomy & Astrophysics*, 355:L27, 2000.

[24] Michael Prouza Martin Jelínek Petr Janeček Jiří Eliášek Jan Ebr, Jiří Blažek. Aerosol measurements using stellar photometry with the fram telescope(s). talk at AtmoHEAD Olomouc, 14. 9. 2016.

[25] Janeček, P., Prouza, M., and Ebr, J. Fram for cta. *EPJ Web of Conferences*, 89:03006, 2015. URL: `https://doi.org/10.1051/epjconf/20158903006`, `doi:10.1051/epjconf/20158903006`.

[26] D. G. Kaskaoutis, H. D. Kambezidis, N. Hatzianastassiou, P. G. Kosmopoulos, and K. V. S. Badarinath. Aerosol climatology: dependence of the angstrom exponent on wavelength over four aeronet sites. *Atmospheric Chemistry and Physics Discussions*, 7:7347–7397, 2007. URL: `https://www.atmos-chem-phys-discuss.net/7/7347/2007/`, `doi:10.5194/acpd-7-7347-2007`.

[27] P. Leonard and N. Gehrels. A history of gamma-ray astronomy including related discoveries. `https://heasarc.gsfc.nasa.gov/docs/history/`, Nov 2009. Online; accessed: 2017-01-08.

[28] Jan Ebr Ivana Ebrová Petr Janeček Martin Jelínek Petr Kubánek Michael Prouza, Jakub Černý and Martin Mašek. Fram – the optical telescope for atmospheric monitoring. 2012.

[29] NASA. The burst and transient source experiment. `https://heasarc.gsfc.nasa.gov/docs/cgro/batse/`. Online; accessed: 2017-01-08.

[30] NASA. The cgro mission (1991 - 2000). `https://heasarc.gsfc.nasa.gov/docs/cgro/index.html`. Online; accessed: 2017-01-08.

[31] NASA. The energetic gamma ray experiment telescope (egret). `https://heasarc.gsfc.nasa.gov/docs/cgro/egret/`. Online; accessed: 2017-01-08.

[32] Anthony L. Peratt. Plasma universe: where is it not? `http://plasmauniverse.info/NoPlasma.html`. Online; accessed: 2017-01-08.

[33] Donald H. Perkins. *Particle astrophysics*. Oxford Univ. Press, 2011.

[34] Jiří Blažek Michael Prouza Martin Mašek Petr Janeček, Jan Ebr and Jiří Eliášek. Fram for the cherenkov telescope array: an update. 2016.

[35] Assignment Point. Assignment on solar radiation. `http://www.assignmentpoint.com/other/assignment-on-solar-radiation.html`. Online; accessed: 2017-01-08.

[36] Michael Prouza. *Ultra-high Energy Cosmic Rays and Theirs Detection in AUGER Project*. PhD thesis, Charles University Prague, 2003.

[37] Maurizio Spurio. *Particles and astrophysics: a multi-messenger approach*. Springer, 2015.

[38] T. Kifune, et al. Very high energy gamma rays from PSR 1706-44. *apjl*, 438:L91–L94, January 1995. `arXiv:astro-ph/9412091`, `doi:10.1086/187723`.

[39] C Toledano, Victoria Cachorro, Alberto Berjón, A Frutos Baraja, Mar Sorribas, Benito Morena, and P Goloub. Aerosol optical depth and Ångström exponent climatology at el arenosillo aeronet site (huelva, spain). 133:795 – 807, 04 2007.

[40] Heinrich J. Völk and Konrad Bernlöhr. Imaging very high energy gamma-ray telescopes. *Experimental Astronomy*, 25(1):173–191, Aug 2009. URL: `https://doi.org/10.1007/s10686-009-9151-z`, `doi:10.1007/s10686-009-9151-z`.

[41] Michal Vraštil. Atmospheric calibration for the cherenkov telescope array. 2016.

[42] A. A. Watson. The discovery of Cherenkov radiation and its use in the detection of extensive air showers. *Nuclear Physics B Proceedings Supplements*, 212:13–19, March 2011. `arXiv:1101.4535`, `doi:10.1016/j.nuclphysbps.2011.03.003`.

[43] National weather service. Layers of the atmosphere. `http://www.srh.noaa.gov/jetstream/atmos/layers.html`. Online; accessed: 2017-01-08.

[44] G. T. Zatsepin and V. A. Kuz'min. Upper Limit of the Spectrum of Cosmic Rays. *Soviet Journal of Experimental and Theoretical Physics Letters*, 4:78, August 1966.

List of Abbreviations

AGN   Active alactic nuclei
AOD   Aerosol optical depth
ASTRI   Astrofisica con Specchi a Tecnologia Replicante Italiana
BATSE   Burst and Transient Source Experiment
BVRI   Blue – Visual – Red – Infrared
CCD   Charge-coupled device
CEILAP   Laser and Applications Research Center
CGRO   Compton Gamma Ray Observatory
CMB   Cosmic microvawe background
CTA   Cherenkov Telescope Array
EAS   Extensive air shower
EGRET   Energetic Gamma Ray Experiment Telescope
ESO   European Organisation for Astronomical Research in the Southern Hemisphere
ESA   The European Space Agency
FRAM   F/(Ph)otometric Robotic Atmospheric Monitor
FoV   Field if view
GBM   Gamma-ray Burst Monitor
GRB   Gamma ray burst
GZK   Greisen-Zatsepin-Kuzmin
HEGRA   High Energy Gamma Ray Astronomy
H.E.S.S.   High Energy Stereoscopic System
HiRes   High Resolution Fly's Eye
IACT   Imaging Atmospheric Cherenkov Telescopes
IFAE   Institut de Física d'Altes Energies
LAT   Greisen-Zatsepin-Kuzmin
LIDAR   Light Detection And Ranging
LST   Large-Size Telescope
LUPM   Laboratoire Univers et Particules de Montpellier
MAGIC   Major Atmospheric Gamma Imaging Cherenkov Telescopes
MC   Monte Carlo
MST   Medium-Size Telescope
NASA   National Aeronautics and Space Administration
OD   Optical depth
PSR   Pulsar
RMS   Root mean square
RTS2   Remote Telescope System, 2nd Version
SNR   Ssupernova remnants
StS   Shoot-the-Shower
UAB   Universitat Autònoma de Barcelona
UBVRI   Ultraviolet – Blue – Visual – Red - Infrared
UHECR   Ultra-high-energy cosmic ray
VAOD   Vertical aerosol optical depth
VERITAS   Very Energetic Radiation Imaging Telescope Array System
VHE   Very high energy

|	
B, B_Tycho	color indices, blue
c	correction constant, system parameter
J	apparent flux
k	extinction coefficient
k_c	correction constant, system parameter
k_M, k_R	extinction coefficient – for Mie, Rayleigh scattering
$m_\text{cat}, m_\text{fit}, m_\text{obs}$	intensity of light – catalog, fitted, observed
M	correction constant, system parameter
n	number of stars
r	distance from the identified light source to the image center
R	correction constant, system parameter
V, V_Tycho	color indices, visual
X	airmass
Z_i	zero-point
β	turbidity coefficient
γ	Ångström coefficient
Θ_Z	zenith angle
λ	wavelength
Λ	Rayleigh attenuation length
$\tau, \tau_\text{M}, \tau_\text{Ray}$	optical depth – general, molecular, caused by Rayleigh scattering
$\omega_\text{J}^2, \omega_\text{M}^2, \omega_\text{star}^2$	uncertainty of measurement – flux, magnitude, whole star

List of Figures

Attachment A

Figure 5.23: Calculated VAOD for data observed in February 2016.
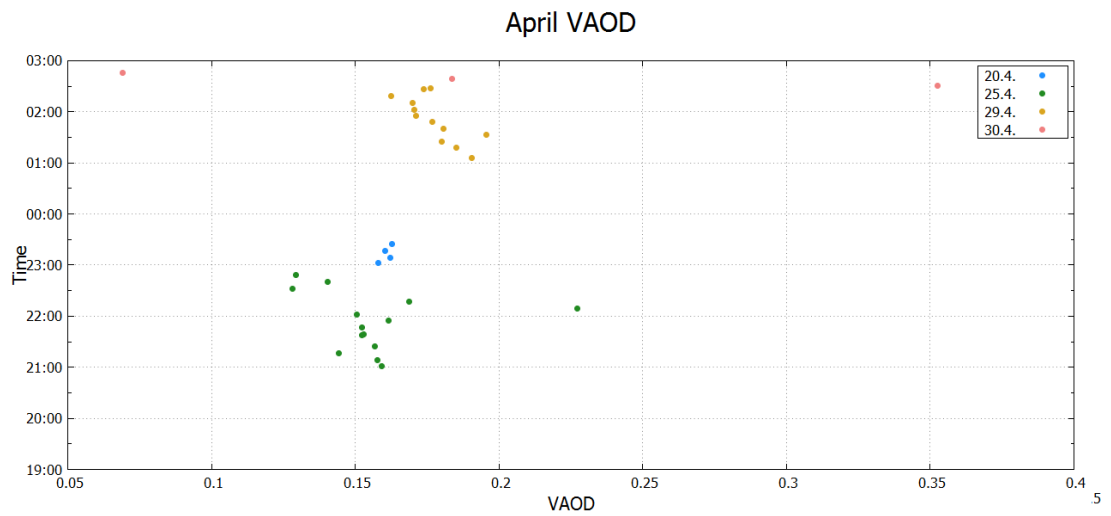
Figure 5.24: Calculated VAOD for data observed in April 2016.
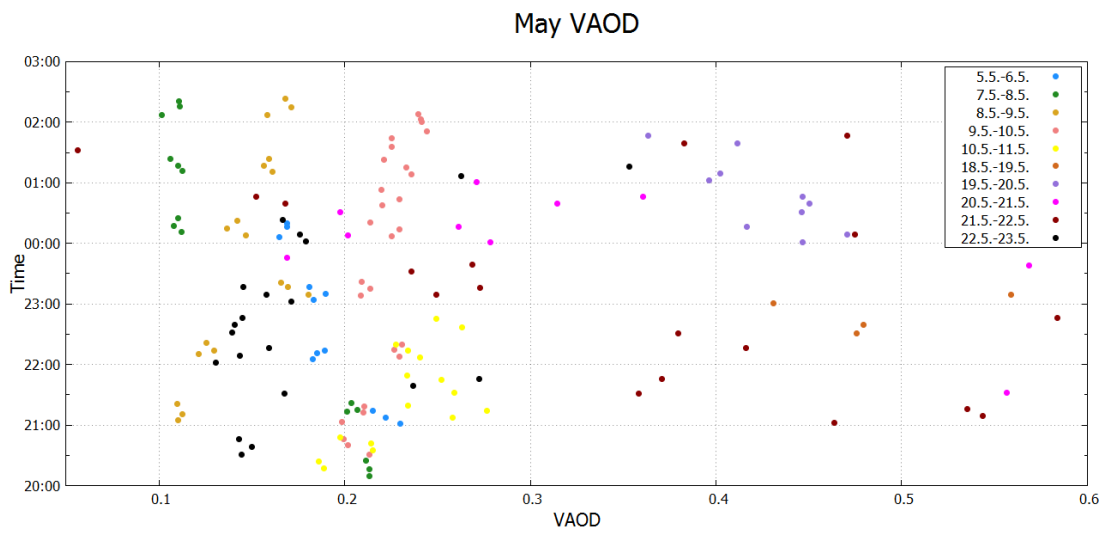
Figure 5.25: Calculated VAOD for data observed in May 2016.
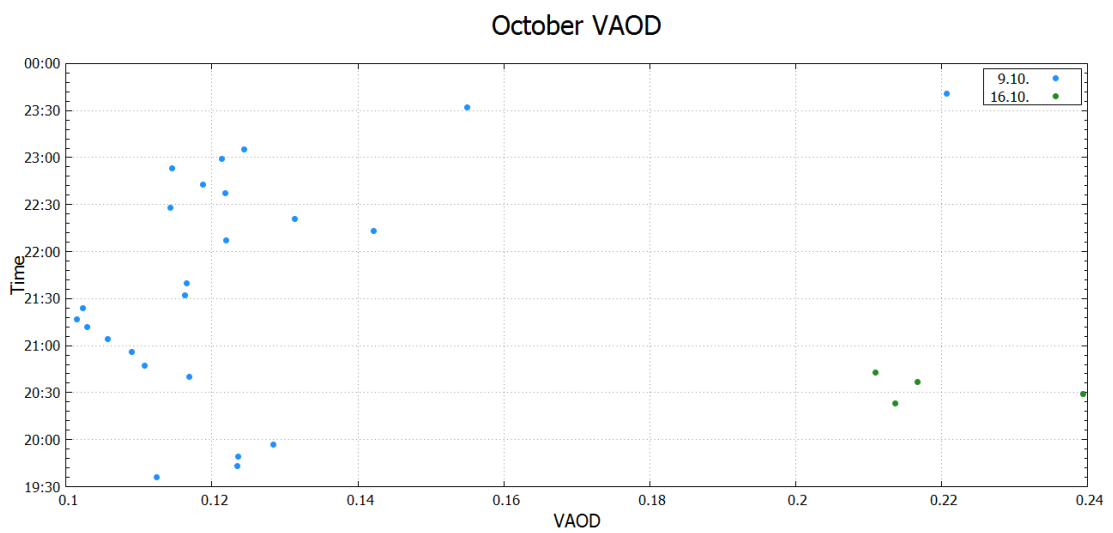
Figure 5.26: Calculated VAOD for data observed in October 2016.
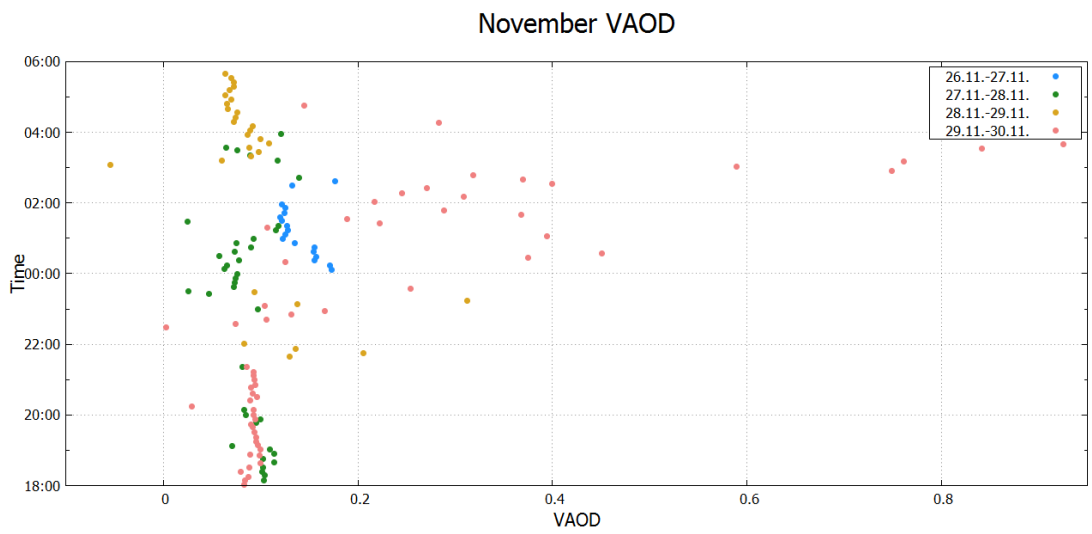
Figure 5.27: Calculated VAOD for data observed in November 2016.
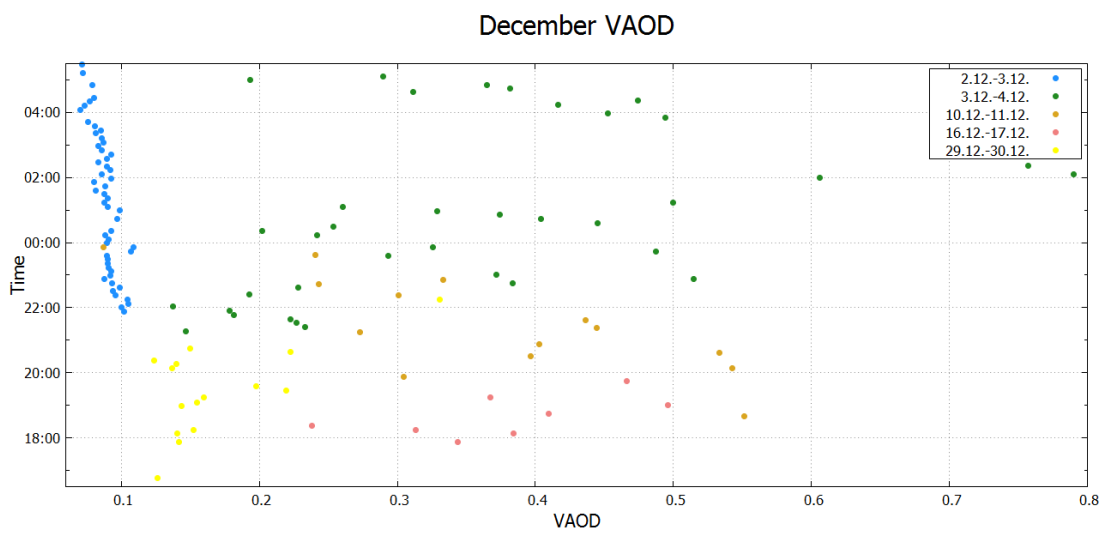
Figure 5.28: Calculated VAOD for data observed in December 2016.
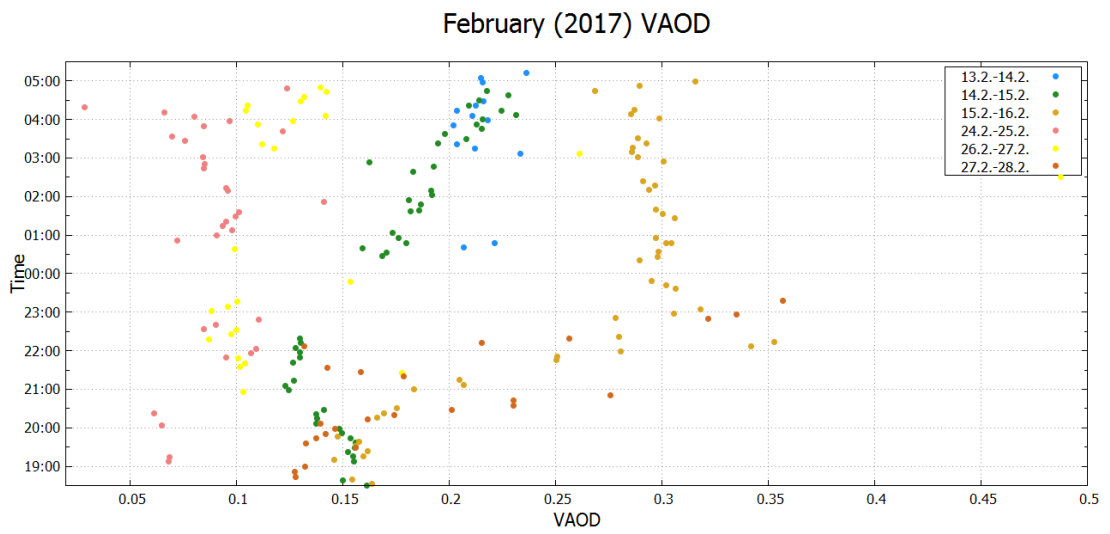
Figure 5.29: Calculated VAOD for data observed in February 2017.
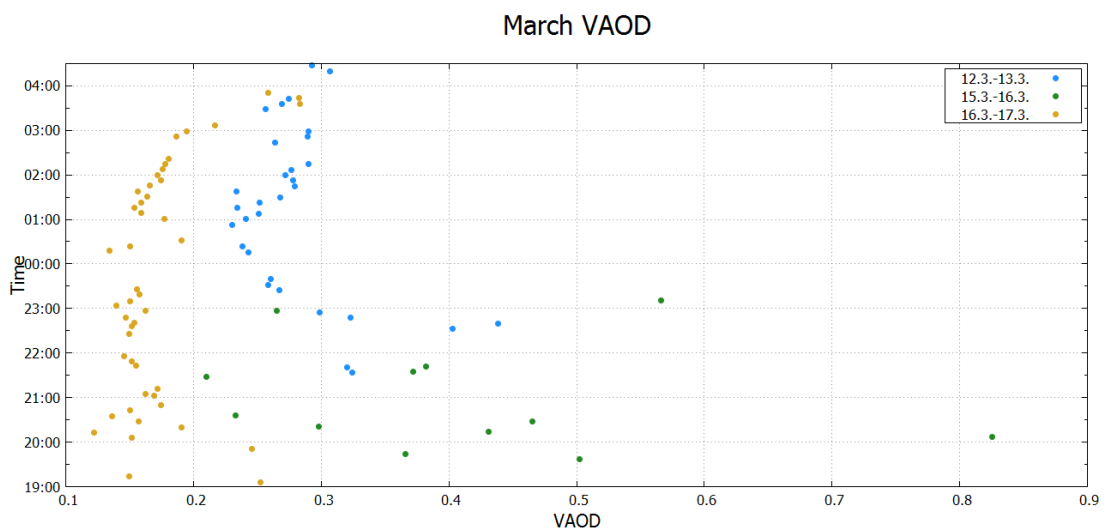
Figure 5.30: Calculated VAOD for data observed in March 2017.

Attachment B

VAOD value usually changes quickly and we need to monitor its development over the course of a whole night. However, it can be useful to know its mean value for approximate estimation of local conditions.

Table 5.1: Mean VAOD values of all observing nights.

2016		2017	
date	**VAOD**	**date**	**VAOD**
24. - 25.2.	0.2 ± 0.1	10. - 11.1.	0.228 ± 0.024
25. - 26.2	0.162 ± 0.026	19. - 20.1.	0.45 ± 0.13
27. - 28.2.	0.29 ± 0.03	20. - 21.1.	0.26 ± 0.04
		26. - 27.1.	0.151 ± 0.017
19. - 20.4.	0.1608 ± 0.0019	27. - 28.1.	0.41 ± 0.14
25. - 26.4.	0.156 ± 0.023	29. - 30.1.	0.6 ± 0.1
28. - 29.4.	0.178 ± 0.009		
29. - 30.4.	0.20 ± 0.12	13. - 14.2.	0.215 ± 0.010
		14. - 15.2.	0.17 ± 0.04
5. - 6.5.	0.190 ± 0.021	15. - 16.2.	0.26 ± 0.07
7. - 8.5.	0.15 ± 0.05	24. - 25.2.	0.089 ± 0.021
8. - 9.5.	0.146 ± 0.023	26. - 27.2.	0.14 ± 0.08
9. - 10.5.	0.222 ± 0.013	27. - 28.2.	0.19 ± 0.07
10. - 11.5.	0.233 ± 0.027		
18. - 19.5.	0.49 ± 0.05	12. - 13.3.	0.28 ± 0.05
19. - 20.5.	0.43 ± 0.03	15. - 16.3.	0.41 ± 0.17
20. - 21.5.	0.7 ± 0.4	16. - 17.3.	0.17 ± 0.04
21. - 22.5.	0.39 ± 0.18		
22. - 23. 5.	0.20 ± 0.12		
9. - 10.10.	0.123 ± 0.024		
16. - 17.10.	0.220 ± 0.012		
26. - 27.11.	0.140 ± 0.020		
27. - 28.11.	0.087 ± 0.025		
28. - 29.11.	0.09 ± 0.06		
29. - 30.11.	0.21 ± 0.21		
2. - 3.12.	0.089 ± 0.009		
3. - 4.12.	0.35 ± 0.16		
10. - 11.12.	0.34 ± 0.15		
16. - 17. 12.	0.38 ± 0.08		
29. - 30. 12.	0.17 ± 0.06		